Generalized parton distributions of the pion in chiral quark models and their QCD evolution

Wojciech Broniowski,[1,2,*] Enrique Ruiz Arriola,[3,†] and Krzysztof Golec-Biernat[1,4,‡]

[1]*The H. Niewodniczański Institute of Nuclear Physics, PL-31342 Kraków, Poland*

[2]*Institute of Physics, Świętokrzyska Academy, ul. Świętokrzyska 15, PL-25406 Kielce, Poland*

[3]*Departamento de Física Atómica, Molecular y Nuclear, Universidad de Granada, E-18071 Granada, Spain*

[4]*Institute of Physics, Rzeszòw University, PL-35959 Rzeszów, Poland*

(Received 6 December 2007; published 27 February 2008)

We evaluate generalized parton distributions of the pion in two chiral quark models: the spectral quark model and the Nambu–Jona-Lasinio model with a Pauli-Villars regularization. We proceed by the evaluation of double distributions through the use of a manifestly covariant calculation based on the α representation of propagators. As a result polynomiality is incorporated automatically and calculations become simple. In addition, positivity and normalization constraints, sum rules, and soft-pion theorems are fulfilled. We obtain explicit formulas, holding at the low-energy quark-model scale. The expressions exhibit no factorization in the t-dependence. The QCD evolution of those parton distributions is carried out to experimentally or lattice accessible scales. We argue for the need of evolution by comparing the parton distribution function and the parton distribution amplitude of the pion to the available experimental and lattice data, and confirm that the quark-model scale is low, about 320 MeV.

DOI: 10.1103/PhysRevD.77.034023 PACS numbers: 12.38.Lg

I. INTRODUCTION

Generalized parton distributions (GPD's) encode detailed dynamical information on the internal structure of hadrons and have thus become in recent times a major theoretical and experimental endeavor (for extensive reviews see, e.g., [1–8] and references therein). They represent a natural interpolation between form factors and quark distribution functions. Actually, while form factors and distribution functions provide in a separate way the spatial and momentum quark distributions in a hadron, respectively, GPD's provide a simultaneous phase-space description of the quark hadron content as far as the position-momentum uncertainty relations allow [5,9]. Experimentally, GPD's show up in hard exclusive processes such as deeply virtual Compton scattering (DVCS) or hard electroproduction of mesons. Factorization for hard exclusive electroproduction of mesons in QCD was proved in Ref. [10]. Effects of the Regge exchanges to exclusive processes were investigated in Ref. [11].

In the present paper we are interested in GPD's for the pion. Although there is little chance of measuring them directly in experiment, the pion GPD's are amenable to indirect experimental determination as well as studies both on transverse [12] as well as Euclidean [13] lattices (for a combination of experimental and lattice-based reconstruction in the proton case see, e.g., Ref. [14]). In addition, there are many theoretical advantages for studying this quark-antiquark bound state. In the first place, in the chiral limit where the current quark masses vanish, the spontaneous breakdown of chiral symmetry of the QCD vacuum generates pions as the zero modes. Their properties are expected to be dominated by the broken chiral symmetry while confinement effects are expected not to be crucial. Actually, finite mass corrections to GPD's of the pion have been treated in the standard [15] and partially-quenched [16] chiral perturbation theory, while the breakdown of the expansion for small $x \sim m_\pi^2/(4\pi f)^2$ has been pointed out in Ref. [17]. Besides, compared to the nucleon there are no spin complications for the pion case, and thus the study reduces to two single scalar GPD functions, one for each isospin combination. Finally, the pion provides a useful framework to learn on the interplay between the chiral symmetry and the light-cone features, since we are studying the behavior of the would-be Goldstone boson in the infinite momentum frame.

Despite the intrinsic complexity of the GPD's, there are a number of simple conditions which ultimately are consequences of the Poincaré and electromagnetic gauge invariance and provide *a priori* tests on the validity of theoretical calculations. Proper support and polynomiality restrictions on the GPD moments [1] are manifestations of the Lorentz invariance. We note that polynomiality is not satisfied in light-front calculations. Double distributions do not suffer from this problem [18] (using the double distributions is a way of *projecting* the Lorentz-violating term onto the right space) although they require the so-called D-terms [19] to comply with the most general polynomial allowed by the dimensional analysis. Normalization conditions and sum rules are a manifestation of the gauge invariance, which at the quark level requires the correct implementation of the electromagnetic Ward-Takahashi identities. The positivity bound [20,21] underlines the Hilbert-space quantum-mechanical probabilistic nature of pion light-cone wave functions, and may impose relevant constraints on admissible regularizations based mainly on

*Wojciech.Broniowski@ifj.edu.pl
†earriola@ugr.es
‡golec@ifj.edu.pl

subtractions of ultraviolet divergences. Soft-pion theorems based on partial conservation of the axial current (PCAC) relate GPD's to parton distribution amplitudes (PDA's) [22]. On a theoretical level, the amazing aspect of GPD's is that the constraints that ought to be fulfilled *a priori* are so demanding and intricate that it is extremely difficult to provide Ansätze fulfilling all of them simultaneously. This is why dynamical calculations going beyond reasonable but admittedly *ad hoc* parametrizations are particularly interesting and instructive. On the other hand, dynamical models providing GPD's are also generating mutually consistent parton distribution functions, parton distribution amplitudes, and form factors. Although this may appear a rather trivial statement, it imposes demanding and tight constraints on details of the calculation, and more specifically on the proper handling of ultraviolet divergences based on the correct implementation of electromagnetic and chiral Ward-Takahashi identities. Even in the case of a simple hadron such as the pion in the chiral limit, the above mentioned necessary conditions provide powerful limitations and in some cases clash with well established prejudices about the meaning and realization of relativistic bound-state wave functions in quantum field theory [23–25].

In the present work we determine GPD's incorporating all the desirable properties required by the symmetries in two chiral quark models, the Nambu–Jona-Lasinio (NJL) model (for reviews see, e.g., [26,27] and references therein) and the spectral quark model (SQM) [28,29], which essentially is a way of introducing regularization in such a way that the vector-meson dominance is built in. These field theoretical models incorporate the spontaneous breaking of chiral symmetry. Chiral quark models use the large-N_c expansion at leading order, where the observables are obtained with one-loop quark diagrams. The present calculation extends previous calculations of parton distribution functions (PDF's) [23,28,30] and PDA's [27,31]. Diagonal GPD in impact-parameter space in these models were considered [32]. Our present GPD result reproduces consistently all these particular cases. Recently, the transition distribution amplitude [33,34] has also been evaluated in SQM [35].

There have been a number of calculations of GPD's and related quantities of the pion within the framework incorporating chiral symmetry. Early calculations of pion GPD's were done in an instanton-inspired model characterized by a momentum-dependent mass function of a dipole form [19,36,37], while PDF's were evaluated in the same model in [38,39]. The crossing-related 2πgeneralized parton amplitude was also evaluated in Ref. [40] in the same instanton model disregarding the momentum dependence of the quark mass, a valid assumption in the limit of small instantons. In that limit, end-point discontinuities arise. A full consideration of poles in the complex plane in a nonlocal version of the NJL model was described in Ref. [41]. Generally, the nonlocality of the quark mass function generated incorrect normalization, since as noted later, PCAC should be properly incorporated [42], an issue also emphasized more recently in Ref. [43]. A rather interesting feature of Ref. [42] is that end-point discontinuities reappear after PCAC is incorporated, even for momentum-dependent quark mass functions, against the widely spread prejudice that they only arise for momentum-independent masses. The operator product expansion and duality aspects of GPD's have been discussed in Ref. [44]. Light-front calculations have been undertaken in Refs. [45,46] for point couplings with subsequent insertion of Gaussian wave functions, however the approach violates polynomiality. Power-law wave functions and GPD's of the pion proposed in Ref. [47] satisfy polynomiality but violate positivity (see [48]). Studies paying particular attention to polynomiality were first made by Tiburzi and Miller [48,49] who proceeded via double distributions [50]. However, regularization in these works was done by introducing momentum-dependent form factors, which makes them difficult to reconcile with the gauge invariance. The model of Ref. [51] based on a pseudoscalar pion-quark coupling does not incorporate chiral symmetry and does not fulfill the momentum sum rule. Noguera, Theußl, and Vento carried out a calculation in the NJL model based on the light-front coordinates, where the fulfillment of polynomiality for nonvanishing momentum transfer is not apparent analytically [52], and in fact numerical integration was required to establish this property. Our NJL results agree with that work, with the important methodological difference that the double distributions, where polynomiality is manifest, are used throughout. Moreover, our regularization is somewhat different than in the model of Ref. [52]; we also use the nonlinear rather than linear realization of the chiral field.

Despite the numerous model calculations of the GPD's, it remains to date unclear what is their significance or impact on the interpretation of actual experiments and/or lattice data. This is, perhaps, why most calculations of the GPD's based on dynamical quark models and going beyond just phenomenological parametrizations do not address this issue. However, while experimental or lattice results generate scale-dependent GPD's, embodying the well established logarithmic scaling violations in QCD, it is notorious that models generally produce scale-independent functions. Thus, quark models represent those distributions at a *given* low energy scale. It is noteworthy that scaling violations can only be computed in the twist expansion order by order. For instance, for the structure functions $F(x, Q)$ with the Bjorken x and momentum Q one has for the quark model

$$F(x, Q) = F_0(x) + \frac{F_2(x)}{Q^2} + \ldots, \tag{1.1}$$

while for QCD

$$F(x, Q) = F_0(x, \alpha(Q^2)) + \frac{F_2(x, \alpha(Q^2))}{Q^2} + \ldots, \quad (1.2)$$

where $F_n(x, \alpha(Q^2))$ are low-energy matrix elements with computable anomalous dimensions and depending logarithmically on the scale through the running coupling constant

$$\alpha(Q^2) = \frac{4\pi}{\beta_0 \log(Q^2/\Lambda^2_{\rm QCD})}, \quad (1.3)$$

$$\beta_0 = \frac{11}{3} N_c - \frac{2}{3} N_f. \quad (1.4)$$

In this work we take

$$\Lambda_{\rm QCD} = 226 \text{ MeV} \quad (1.5)$$

and $N_c = N_f = 3$. The matching conditions are taking at a given scale Q_0 order by order in the twist expansion

$$F_n(x)|_{\rm Model} = F_n(x, \alpha(Q_0^2))|_{\rm QCD}. \quad (1.6)$$

A quite different issue is the operational definition of the low-energy reference scale Q_0. Here we will use along the lines of previous works [23,27,30,31] the momentum fraction carried by the valence quarks. It turns out that in order to describe the available pion phenomenology the initial scale Q_0 from the quark model must be very low, around 320 MeV. At such low scale the perturbative expansion parameter in the evolution equations is large, $\alpha(Q_0^2)/2\pi = 0.34$, which makes the evolution very fast for scales close to the initial value Q_0.

None of the previous chiral-quark-model studies of the genuine GPD's (off-forward nondiagonal) carried out the QCD evolution, starting from the initial condition provided by the models. The evolution is a major element of this work. As already mentioned, it is also a crucial element if one wishes to compare the model prediction to the data from experiments or lattice simulations. At the moment these data are available only for the forward diagonal parton distribution function of the pion, or the PDA.

We have taken an effort to separate formal aspects of the calculation from the model-dependent technicalities of the regularization. That way we simply achieve the desired features on general grounds, such as the sum rules or the polynomiality conditions [1]. We stress this is achieved without a factorized form in the t variable. In one of the considered models (the spectral quark model) the final results for the GPD's can be written in terms of rather simple but nontrivial analytic formulas, which allows for more insight into their properties. We also show that our GPD's satisfy the positivity bounds. In essence, all the known consistency conditions and constraints are indeed satisfied in our calculation.

The outline of the paper is as follows: In Sec. II we list the definitions and properties of the GPD's. We introduce both the asymmetric and symmetric kinematics, as well as define the isospin projections. We give the generic quark-model expressions in terms of the two- and three-point functions. Sections III and IV contain the results of the spectral quark model and the NJL model, respectively. We discuss the general need for the QCD evolution of chiral quark models in Sec. V, where we define the matching condition in the light of phenomenological analyses, as well as Euclidean and transverse lattice calculations. In particular, we show the evolved forward diagonal PDF of the pion and confront it with the results of the E615 experiment at Fermilab [53]. This agreement is quite remarkable, but sets the quark model momentum scale to very low values, $Q_0 \simeq 320$ MeV. Likewise we also discuss the evolved PDA as compared to the E791 measurement [54] of the pion light-cone wave function and to the lattice data. We show how the QCD evolution leads to vanishing of the PDF at $x = 1$ and of the PDA at $x = 0, 1$, which is the desired end-point behavior. The LO QCD evolution of our genuine GPD's, based on the standard ERBL-DGLAP equations, is carried out in Sec. VI, where the obtained quark-model initial conditions are evolved to higher momentum scales. Finally, in Sec. VII we draw our main conclusions. The appendices contain the technique of analyzing the GPD's through the use of the α representation for the propagators. This method, first introduced in the context of structure functions in Refs. [38,39], allows for a manifestly covariant calculation and leads to simple formal expressions for the basic two- and three-point functions emerging in the analysis. The appearance of D-terms is manifest and natural in this treatment, based solely on the Feynman diagrams in a conventional way. We also list explicitly the basic two- and three-point functions of the two considered model. We proceed via the double distributions, which leads to a simple proof of polynomiality [2].

II. DEFINITIONS AND QUARK-MODEL EXPRESSIONS

A. Formalism for pion GPD

The kinematics of the process and the assignment of momenta (in the asymmetric way) is displayed in Figs. 1 and 2. For the pions on the mass shell we have, adopting the standard notation,

$$p^2 = m_\pi^2, \qquad q^2 = -2p \cdot q = t, \qquad n^2 = 0, \qquad p \cdot n = 1, \qquad q \cdot n = -\zeta. \quad (2.1)$$

Note the sign convention for t, positive in the physical region.

The leading-twist off-forward ($t \neq 0$) nondiagonal ($\zeta \neq 0$) GPD of the pion is defined as

$$\mathcal{H}^{ab}(x, \zeta, t) = \int \frac{dz^-}{4\pi} e^{ixp^+z^-} \langle \pi^b(p+q)|\bar{\psi}(0)\gamma \cdot nT\psi(z)|\pi^a(p)\rangle|_{z^+=0, z^\perp=0}, \quad (2.2)$$

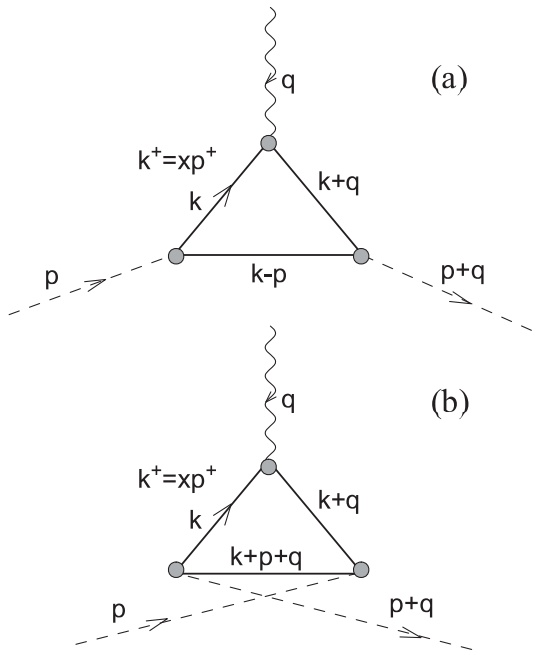

FIG. 1. The direct (a) and crossed (b) Feynman diagrams for the quark-model evaluation of the GPD of the pion.

where $0 \leq \zeta$ and the x variable, $-1+\zeta \leq x \leq 1$, is defined in the *asymmetric* notation (cf. Fig. 1), a and b are isospin indices for the pion, T is the isospin matrix equal 1 for the isoscalar and τ_3 for the isovector cases, finally ψ is the quark field and z is the light-cone coordinate. Explicitly, the two isospin projections are equal to

$$\delta_{ab}\mathcal{H}^{I=0}(x,\zeta,t) = \int \frac{dz^-}{4\pi} e^{ixp^+z^-} \langle \pi^b(p+q)|\bar{\psi}(0)\gamma \cdot n\psi(z)|\pi^a(p)\rangle|_{z^+=0,z^\perp=0}, \tag{2.3}$$

$$i\epsilon_{3ab}\mathcal{H}^{I=1}(x,\zeta,t) = \int \frac{dz^-}{4\pi} e^{ixp^+z^-} \langle \pi^b(p+q)|\bar{\psi}(0)\gamma \cdot n\psi(z)\tau_3|\pi^a(p)\rangle|_{z^+=0,z^\perp=0}. \tag{2.4}$$

One can form the combinations termed the quark and antiquark GPD's of the pion,

$$\mathcal{H}_q(x,\zeta,t) = \frac{1}{2}(\mathcal{H}_{I=0}(x,\zeta,t) + \mathcal{H}_{I=1}(x,\zeta,t)),$$
$$\mathcal{H}_{\bar{q}}(x,\zeta,t) = \frac{1}{2}(\mathcal{H}_{I=0}(x,\zeta,t) - \mathcal{H}_{I=1}(x,\zeta,t)). \tag{2.5}$$

From the general formulation it follows that $\mathcal{H}_q(x,\zeta,t)$ has the support $x \in [0,1]$, whereas $\mathcal{H}_{\bar{q}}(x,\zeta,t)$ the support $x \in [-1+\zeta,\zeta]$. The range $x \in [0,\zeta]$ is called the Efremov-Radyushkin-Brodsky-Lepage (ERBL) region, while $x \in [-1+\zeta,0]$ and $x \in [\zeta,1]$ are the Dokshitzer-Gribov-Lipatov-Altarelli-Parisi (DGLAP) regions, where the nomenclature refers to the QCD evolution; see Sec. VI.

In the *symmetric* notation, somewhat more convenient in certain applications,[1] one introduces

$$\xi = \frac{\zeta}{2-\zeta}, \qquad X = \frac{x-\zeta/2}{1-\zeta/2}, \tag{2.6}$$

where $0 \leq \xi \leq 1$ and $-1 \leq X \leq 1$. Then

$$H^{I=0,1}(X,\xi,t) = \mathcal{H}^{I=0,1}\left(\frac{\xi+X}{\xi+1}, \frac{2\xi}{\xi+1}, t\right) \tag{2.7}$$

with the symmetry properties about the $X=0$ point,

$$H^{I=0}(X,\xi,t) = -H^{I=0}(-X,\xi,t),$$
$$H^{I=1}(X,\xi,t) = H^{I=1}(-X,\xi,t). \tag{2.8}$$

The following sum rules hold:

$$\int_{-1}^{1} dX H^{I=1}(X,\xi,t) = 2F_V(t), \tag{2.9}$$

$$\int_{-1}^{1} dX X H^{I=0}(X,\xi,t) = \theta_2(t) - \xi^2\theta_1(t), \tag{2.10}$$

where $F_V(t)$ is the electromagnetic form factor, while $\theta_1(t)$ and $\theta_2(t)$ are the gravitational form factors of the pion (see Appendix D) which satisfy the low-energy theorem $\theta_1(0) = \theta_2(0)$ in the chiral limit [55]. Sum rule (2.9) expresses the electric charge conservation, while (2.10) is responsible for the momentum sum rule in deep inelastic scattering. Finally, for $X \geq 0$

$$\mathcal{H}^{I=0,1}(X,0,0) = q(X),$$

relating the distributions to the pion's forward diagonal PDF, $q(X)$.

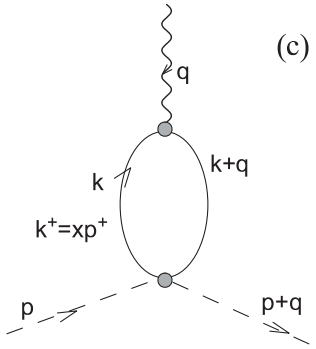

FIG. 2. The contact contribution (c) to the GPD of the pion, responsible for the D-term.

[1] In this paper we switch back and forth between the two conventions, since explicit expressions are shorter in the asymmetric notation, while some formal features are simpler to state in the symmetric notation.

The *polynomiality* conditions [1,2] state that

$$\int_{-1}^{1} dX X^{2j} H^{I=1}(X,\xi,t) = \sum_{i=0}^{j} A_i^{(j)}(t)\xi^{2i},$$
$$\int_{-1}^{1} dX X^{2j+1} H^{I=0}(X,\xi,t) = \sum_{i=0}^{j+1} B_i^{(j)}(t)\xi^{2i}, \tag{2.11}$$

where $A_i^{(j)}(t)$ and $B_i^{(j)}(t)$ are the coefficient functions (form factors) depending on j and i. The polynomiality conditions follow from basic field-theoretic assumptions such as the Lorentz invariance, time reversal, and Hermiticity, hence are automatically satisfied in approaches that obey these requirements. Conditions (2.11) supply important tests of consistency. In our approach the polynomiality will be demonstrated straightforwardly in an analytic way through the use of double distributions; see Appendix A.

Another constraint for the GPD's, the *positivity bound* [21], is derived with the help of the Schwartz inequality and the momentum representation of the pion light-cone wave functions. In the simplest form the constraint states that (for $t \le 0$)

$$|H_q(X,\xi,t)| \le \sqrt{q(x_{\rm in})q(x_{\rm out})}, \qquad \xi \le X \le 1. \tag{2.12}$$

where $x_{\rm in} = (x+\xi)/(1+\xi)$, $x_{\rm out} = (x-\xi)/(1-\xi)$.

The off-forward ($\Delta_\perp \neq \mathbf{0}$) diagonal ($\xi = 0$) GPD of the pion (we take π^+) can be written as

$$H(x,\xi=0,-\Delta_\perp^2) = \int d^2\mathbf{b} e^{i\Delta_\perp\cdot\mathbf{b}} q(x,\mathbf{b}). \tag{2.13}$$

We use here

$$q(x,\mathbf{b}) = \int \frac{dz^-}{4\pi} e^{ixp^+z^-} \langle \pi^+(p')|\bar{q}\Big(0,-\frac{z^-}{2},\mathbf{b}\Big) \times \gamma^+ q\Big(0,\frac{z^-}{2},\mathbf{b}\Big)|\pi^+(p)\rangle, \tag{2.14}$$

where x is the Bjorken x, $\Delta_\perp = p' - p$ lies in the transverse plane, and b is an impact parameter. The model-independent relation found in Ref. [56] reads in the pion case

$$\int_0^1 dx q(x,\mathbf{b}) = \int \frac{d^2\mathbf{q}_\perp}{(2\pi)^2} e^{i\mathbf{q}_\perp\cdot\mathbf{b}} F_V(-\mathbf{q}_\perp^2). \tag{2.15}$$

By crossing, the process related to the DVCS off the pion, i.e., two pion production in $\gamma^*\gamma$ collisions, can be measured at low invariant masses [57]. The relevant matrix element reads

$$\Phi^{ab}(u,\zeta,W^2) = \int \frac{dz^-}{4\pi} e^{ixp^+z^-} \langle \pi^a(p_1)\pi^b(p_2)|\bar{\psi}(0)\gamma \cdot nT\psi(z)|0\rangle|_{z^+=0,z^\perp=0}, \tag{2.16}$$

where $W^2 = (p_1+p_2)^2$, $\zeta = p_1\cdot n/P\cdot n$, and $u = (p_1 - p_2)^2$. By comparing, we have

$$\Phi^{ab}(u,\zeta,W^2) = \mathcal{H}^{ab}(x,\zeta,t). \tag{2.17}$$

One has the *soft-pion theorem* [22],

$$\Phi^{I=1}(u,1,0) = H^{I=1}(2u-1,1,0) = \phi(u), \tag{2.18}$$

where $\phi(u)$ represents the PDA defined as

$$\langle \pi^a(p)|\bar{\psi}(z)\gamma^\mu\gamma_5\frac{1}{2}\tau^b\psi(0)|0\rangle|_{z^+=0,z^\perp=0} = ifp^\mu\delta^{ab}\int_0^1 dx e^{ixp\cdot z}\phi(x). \tag{2.19}$$

Note that result (2.18) is based on PCAC and hence is a consequence of the chiral symmetry. One of the reasons to prefer GPD's rather than 2πPDA is the absence of final state interactions, which are suppressed in the large N_c limit.[2]

B. Formal results for chiral quark models

The reduction formulas applied to the definition (2.4) result in the amputated three-point Green function with the constrained quark momentum integration, $k^+ = xp^+$. Large-N_c treatment leads to one-quark-loop diagrams, with massive quarks due to spontaneous chiral symmetry breaking. In *nonlinear* chiral quark models the quark-pion interaction is described by the term $-\bar{\psi}\omega U^5\psi$ in the effective action, where the pion field matrix is

$$U^5 = \exp(i\gamma_5\tau\cdot\phi/f), \tag{2.20}$$

where f denotes the pion decay constant. The resulting Feynman rules and the definition (2.2) lead to the Feynman diagrams of Figs. 1 and 2.[3] The presence of the contact term is crucial for the preservation of the chiral symmetry [19]. The evaluation of the diagrams is straightforward, giving the following result for the isosinglet and isovector parts:

$$\mathcal{H}_{I=0}(x,\zeta,t) = \mathcal{H}_a(x,\zeta,t) + \mathcal{H}_b(x,\zeta,t) + \mathcal{H}_c(x,\zeta,t),$$
$$\mathcal{H}_{I=1}(x,\zeta,t) = \mathcal{H}_a(x,\zeta,t) - \mathcal{H}_b(x,\zeta,t). \tag{2.21}$$

The explicit contributions of the subsequent diagrams to the GPD's of Eq. (2.21) are

[2]The simplest example illustrating this feature is provided by the pion electromagnetic form factor. The radius reads

$$\langle r^2\rangle_\pi = \frac{6}{M_V^2}\Big[1 - \frac{1}{4N_c}\log\Big(\frac{m_\pi^2}{M_V^2}\Big)\Big],$$

the first contribution stemming from the quark loop and the second contribution an estimate from pion loops [58].

[3]The similar calculation of Ref. [52] uses the linear realization of the chiral symmetry, with the σ field present.

$$\mathcal{H}_a(x,\zeta,t) = \frac{iN_c\omega^2}{4\pi^2 f^2}\int d^4k\,\delta(k\cdot n - x)\frac{\omega^2 - k^2 - \zeta(\omega^2 - k^2 + k\cdot p) + x(\omega^2 - \frac{t}{2} - k^2 + 2k\cdot p) - k\cdot q}{D_k D_{k+q} D_{k-p}},$$
$$\mathcal{H}_b(x,\zeta,t) = \frac{iN_c\omega^2}{4\pi^2} f^2\int d^4k\,\delta(k\cdot n - x)\frac{-\omega^2 + k^2 + \zeta k\cdot p + x(\omega^2 - \frac{t}{2} - k^2 - 2k\cdot p - 2k\cdot q) + k\cdot q}{D_k D_{k+q} D_{k+p+q}}, \quad (2.22)$$
$$\mathcal{H}_c(x,\zeta,t) = \frac{iN_c\omega^2}{4\pi^2 f^2}\int d^4k\,\delta(k\cdot n - x)\frac{2x-\zeta}{D_k D_{k+q}}.$$

The denominator of the propagator of quark of mass ω and momentum l is denoted as

$$D_l = l^2 - \omega^2 + i0. \quad (2.23)$$

The powers of the momentum k in the numerators may be eliminated with the following reduction formulas:

$$k^2 = D_k + \omega^2, \qquad k\cdot q = \frac{1}{2}(D_{k+q} - t - D_k),$$
$$k\cdot p = -\frac{1}{2}(D_{k-p} - m_\pi^2 - D_k), \quad (2.24)$$
$$k\cdot p = \frac{1}{2}(D_{k+p+q} - m_\pi^2 - D_{k+q} + t).$$

Then the GPD's become

$$\mathcal{H}_{I=0,1}(x,\zeta,t) = \frac{-iN_c\omega^2}{8\pi^2 f^2}\int d^4k\,\delta(k\cdot n - x) \times\left(\frac{1}{D_k D_{k-p}} + \frac{1-\zeta}{D_{k+q}D_{k-p}} \mp \frac{1}{D_{k+q}D_{k+p+q}} \mp \frac{1-\zeta}{D_k D_{k+p+q}} + \frac{(\zeta-2x)m_\pi^2 + t(x-1)}{D_k D_{k+q} D_{k-p}} \mp \frac{(\zeta-2x)m_\pi^2 + t(x-\zeta+1)}{D_k D_{k+q} D_{k+p+q}}\right), \quad (2.25)$$

with the upper (lower) signs corresponding to the case of $I = 0$ ($I = 1$). Note that the piece with $1/(D_k D_{k+q})$ cancels out due to the presence of contact diagram (c). The contribution of the diagram (c), having the support for $x \in [0, \zeta]$, is the D-term [19].

From the above form it is clear that we need to consider two generic types of two- and three-point integrals:

$$I(x, l\cdot n, l'\cdot n, (l-l')^2) = \frac{-iN_c\omega^2}{4\pi^2 f^2}\int d^4k\frac{\delta(k\cdot n - x)}{D_{k-l}D_{k-l'}},$$
$$J(x, l\cdot n, l'\cdot n, l^2, l'^2, l\cdot l') = \frac{iN_c\omega^2}{4\pi^2 f^2}\int d^4k\frac{\delta(k\cdot n - x)}{D_k D_{k-l} D_{k-l'}}. \quad (2.26)$$

These are analyzed in detail in Appendices A 1 and A 2. The two-point function I is logarithmically divergent, hence the analysis needs regularization. This is where different quark models depart from one another. We may separate the issues of regularization from formal expressions, which is convenient for theoretical aspects and the demonstration of the consistency conditions. Written in terms of the basic two- and three-point functions Eq. (2.25) becomes

$$\mathcal{H}_{I=0,1}(x,\zeta,t) = \frac{1}{2}\Big[I(x,0,1,m_\pi^2) + (1-\zeta)I(x,\zeta,1,m_\pi^2) \mp I(x,-1+\zeta,\zeta,m_\pi^2) \mp (1-\zeta)I(x,-1+\zeta,0,m_\pi^2) - [(\zeta-2x)m_\pi^2 + t(x-1)] \times J\Big[x,\zeta,1,t,m_\pi^2,-\frac{t}{2}\Big] \pm [(\zeta-2x)m_\pi^2 + t(x-\zeta+1)] \times J\Big[\zeta-x,\zeta,1,t,m_\pi^2,-\frac{t}{2}\Big]\Big]. \quad (2.27)$$

This equation may be considered as the generic nonlinear local chiral quark-model result for the isospin-projected GPD's of the pion. Model details, such as regularization, affect the specific form of the two- and three-point functions, but leave the structure of Eq. (2.27) unchanged. The nontrivial features of the regularization will utterly be responsible for the fulfillment of the general properties of GPD's described in Sec. II A.

III. RESULTS OF THE SPECTRAL QUARK MODEL

Now we come to the evaluation of GPD in specific models. From now on we work for simplicity in the chiral limit,

$$m_\pi = 0. \quad (3.1)$$

The first model we consider is the SQM of Ref. [29], where all the necessary details of the model can be found. The one-quark-loop action of this model is

$$\Gamma = -iN_c\int_C d\omega\,\rho(\omega)\,\mathrm{Tr}\log(i\partial\!\!\!/ - \omega U^5), \quad (3.2)$$

where $\rho(\omega)$ is the quark generalized *spectral function*, and U^5 is given in Eq. (2.20). In the calculations of this paper we only need the vector part of the spectral function, which in the *meson-dominance* SQM [29] has the form

$$\rho_V(\omega) = \frac{1}{2\pi i}\frac{1}{\omega}\frac{1}{(1-4\omega^2/M_V^2)^{5/2}}, \quad (3.3)$$

exhibiting the pole at the origin and cuts starting at $\pm M_V/2$, where M_V is the mass of the vector meson, $M_V = m_\rho = 770$ MeV. The contour C for the integration in (3.2) is shown in Fig. 3. Despite the rather unusual appearance of

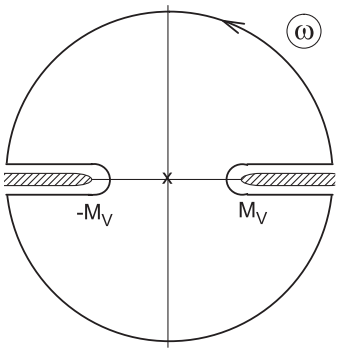

FIG. 3. The contour C for evaluation of observables in the meson-dominance variant of SQM. M_V denotes the ρ-meson mass. The cross and hatched regions indicate the position of the pole and cuts of the spectral function Eq. (3.3).

the spectral function, the model leads to conventional phenomenology [29,59]. Importantly, it implements the vector-meson dominance, yielding the pion electromagnetic form factor of the monopole form

$$F_V^{\mathrm{SQM}}(t) = \frac{M_V^2}{M_V^2 - t}. \tag{3.4}$$

For the gravitational form factor we find

$$\theta_1^{\mathrm{SQM}}(t) = \theta_2^{\mathrm{SQM}}(t) = \frac{M_V^2}{t}\log\left(\frac{M_V^2}{M_V^2 - t}\right) \equiv F_S^{\mathrm{SQM}}(t). \tag{3.5}$$

Both the electromagnetic and gravitational form factors for SQM are plotted in Fig. 4 with solid lines.

With the help of Eq. (B1) and (B8) it is straightforward to obtain the formulas for the GPD's in SQM. The expressions are simple in the chiral limit, and shortest in the asymmetric notation. For the quark and antiquark GPD's we obtain

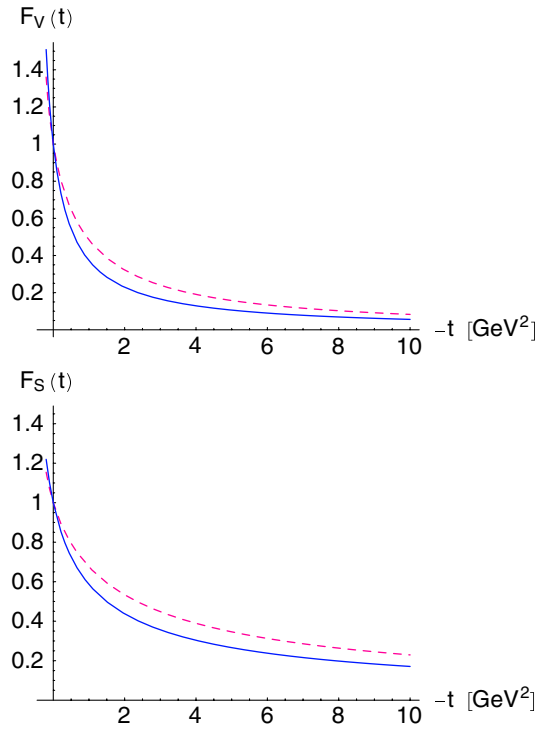

FIG. 4 (color online). The pion electromagnetic, $F_V(t)$, (top) and gravitational, $\theta_1(t) = \theta_2(t) \equiv F_S(t)$, (bottom) form factors in SQM [solid line, Eqs. (3.4) and (3.5)] and in NJL model [dashed line, Eq. (4.3)].

$$\begin{aligned}
2\mathcal{H}_q(x,\zeta,t) &= \theta((1-x)x) + \theta((1-x)(x-\zeta)) + t(1-x) \\
&\times\left[\frac{2(x-1)(t(x-1)^2 + 3(\zeta-1)M_V^2)\theta(1-x)\theta(x-\zeta)}{(t(x-1)^2 + (\zeta-1)M_V^2)^2} + \left(\frac{(x-1)(t(x-1)^2 + 3(\zeta-1)M_V^2)}{(t(x-1)^2 + (\zeta-1)M_V^2)^2}\right.\right. \\
&\left.\left. + \frac{(x(\zeta-2)+\zeta)(3(\zeta-1)\zeta^2 M_V^2 + t((\zeta^2+8\zeta-8)x^2 + 2(4-5\zeta)\zeta x + \zeta^2))}{(\zeta^2 + \frac{4tx(x-\zeta)}{M_V^2})^{3/2}(t(x-1)^2 + (\zeta-1)M_V^2)^2}\right)\theta(x)\theta(\zeta-x)\right], \\
\mathcal{H}_{\bar{q}}(x,\zeta,t) &= \mathcal{H}_q(\zeta - x, \zeta, t).
\end{aligned} \tag{3.6}$$

From these, the isospin combinations are trivial to get. The formulas satisfy the consistency relations (2.8), (2.9), and (2.10). In particular, upon passing to the symmetric notation and using the above formulas we verify

$$\begin{aligned}
\int_{-1}^{1} dX H^{I=1}(X,\xi,t) &= 2F_V^{\mathrm{SQM}}(t), \\
\int_{-1}^{0} dX X H^{I=0}(X,\xi,t) &= (1-\xi^2)F_S^{\mathrm{SQM}}(t).
\end{aligned} \tag{3.7}$$

The isovector norm is decomposed as follows between the ERBL and DGLAP regions:

$$\begin{aligned}
\int_0^{\zeta} dx \mathcal{H}_q(x,\zeta,t) &= \frac{2-\zeta}{2}\frac{M_V^2}{M_V^2 - t} \\
&\times \frac{\zeta(M_V^2 + t(1-\zeta))}{(2-\zeta)(M_V^2 - t(1-\zeta))}, \\
\int_{\zeta}^{1} dx \mathcal{H}_q(x,\zeta,t) &= \frac{2-\zeta}{2}\frac{M_V^2}{M_V^2 - t} \\
&\times \frac{2(1-\zeta)(M_V^2 - t)}{(2-\zeta)(M_V^2 - t(1-\zeta))}.
\end{aligned} \tag{3.8}$$

Some special values of the GPD's in SQM are

$$\begin{aligned}
&\mathcal{H}^{I=1}(1,\zeta,t) = \mathcal{H}^{I=0}(1,\xi,t) = 1,\\
&\mathcal{H}^{I=1}(\zeta,\zeta,t) = \frac{M_V^2(M_V^2 + t(1-\zeta))}{(M_V^2 - t(1-\zeta))^2},\\
&\lim_{x\to\zeta^+}\mathcal{H}^{I=0}(x,\zeta,t) = \frac{M_V^2(M_V^2 + t(1-\zeta))}{(M_V^2 - t(1-\zeta))^2},\\
&\lim_{x\to\zeta^-}\mathcal{H}^{I=0}(x,\zeta,t) = \frac{t(3M_V^2 - t(1-\zeta))(1-\zeta)}{(M_V^2 - t(1-\zeta))^2}.
\end{aligned} \tag{3.9}$$

The values at $x = -1+\zeta$ and $x = 0$ follow from the symmetry relations $\mathcal{H}^{I=1,0}(x,\zeta,t) = \pm\mathcal{H}^{I=1,0}(\zeta - x,\zeta,t)$. We note that the discontinuities at the end points $x = \pm 1$ and for the $I = 0$ part at $x = 0$ and $x = \zeta$ are a typical feature of quark-model calculations. The QCD evolution immediately washes out these discontinuities see Sec. VI. The derivative of $\mathcal{H}^{I=1}(x,\zeta,t)$ with respect to x is continuous at the point $x = \zeta$, where

$$\frac{d}{dx}\mathcal{H}^{I=1}(x,\zeta,t)\,|_{x=\zeta} = -\frac{2M_V^2 t(3M_V^2 + t(1-\zeta))}{(M_V^2 - t(1-\zeta))^3}. \tag{3.10}$$

On general grounds, Eqs. (3.6) also satisfy the polynomiality conditions (2.11), which can be seen from the derivation through the double distributions shown in Appendix A. Also note that the obtained formulas are certainly not of the form where the t-dependence is factorized, i.e.,

$$H^{I=0,1}(X,\xi,t) \neq F(t)G(X,\xi). \tag{3.11}$$

For the case of $t = 0$ the formulas (3.6) simplify to the well-known [19,52] step-function results

$$\begin{aligned}
&\mathcal{H}_{I=0}(x,\zeta,0) = \theta[(1-x)(x-\zeta)] - \theta[-x(x+1-\zeta)],\\
&\mathcal{H}_{I=1}(x,\zeta,0) = \theta[(1-x)(x+1-\zeta)].
\end{aligned} \tag{3.12}$$

Another simple case is for $\zeta = 0$ and any value of t,

$$\mathcal{H}_{\ q}(x,0,t) = \frac{M_V^2(M_V^2 + t(x-1)^2)}{(M_V^2 - t(x-1)^2)^2}, \tag{3.13}$$

which agrees with the result reported in [32]. The corresponding impact-parameter representation obtained there is given by the formula[4]

$$q(x,\mathbf{b}) = \frac{M_V^2}{2\pi(1-x)^2}\times\left[\frac{bM_V}{1-x}K_1\left(\frac{bM_V}{1-x}\right) - K_0\left(\frac{bM_V}{1-x}\right)\right]. \tag{3.14}$$

From this expression one obtains

$$\int_0^1 dx q(x,\mathbf{b}) = \frac{M_V^2 K_0(bM_V)}{2\pi}. \tag{3.15}$$

[4]Note an overall sign missing in Ref. [32].

This complies to the model-independent relation (2.15) when the vector-dominance form factor (3.4) is used, since, explicitly,

$$\int\frac{d^2q}{2\pi}\frac{e^{i\mathbf{q}\cdot\mathbf{b}}}{M_V^2 + \mathbf{q}^2} = K_0(bM_V). \tag{3.16}$$

The case of Eq. (3.6) for $\zeta = 0.5$ and several values of t is shown in Fig. 5. Results for other values of ζ are qualitatively similar. Figure 6 shows the isospin 0 and 1 combinations, $H_{I=0,1}$. We note that the $I = 1$ GPD and its first derivative with respect to x is continuous at $x = 0$ and $x = \zeta$, while the $I = 0$ combination is discontinuous at these points.

At $t = 0$ we have the above-mentioned step-function results

$$\begin{aligned}
H_{I=1} &= \theta(1-X^2),\\
H_{I=0} &= \theta((1-X)(X-\xi)) - \theta((1+X)(-X-\xi)).
\end{aligned} \tag{3.17}$$

As $-t$ increases, the strength moves to the vicinity of the $X = \pm 1$ points. The limit of $-t(1-x)\to\infty$ in Eqs. (3.6) yield the asymptotic forms

$$\begin{aligned}
&\mathcal{H}^{I=1,0}(1,\zeta,t) = 1,\\
&\mathcal{H}^{I=1}(x,\zeta,t) \simeq \frac{M_V^2(1-\zeta)}{t(1-x)^2}, \quad x\in[0,1),\\
&\mathcal{H}^{I=0}(x,\zeta,t) \simeq \frac{M_V^2(1-\zeta)}{t(1-x)^2}, \quad x\in(\zeta,1),\\
&\lim_{x\to\zeta^-}\mathcal{H}^{I=0}(x,\zeta,t) = -1 + \frac{M_V^2}{(1-\zeta)t},\\
&\mathcal{H}^{I=0}(x,\zeta,t) \simeq \frac{M_V^2(2x-\zeta)(\zeta^2 - 3\zeta + 2)}{2(x-1)^2(x-\zeta+1)^2 t}, \quad x\in(0,\zeta).
\end{aligned} \tag{3.18}$$

In the DGLAP region the absolute value of the $I = 0, 1$ functions are bounded by unity. Note that at large $-t$ the

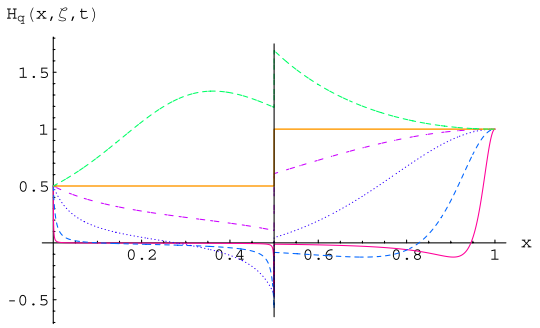

FIG. 5 (color online). The SQM results for the quark GPD of the pion, $\mathcal{H}_{\ q}$ of Eq. (2.5), plotted as a function of x for $\zeta = 1/2$ and $t = 0.2, 0, -0.2, -1, -10, -100$ GeV^2, from top to bottom (at $x = 0.9$). Asymmetric notation.

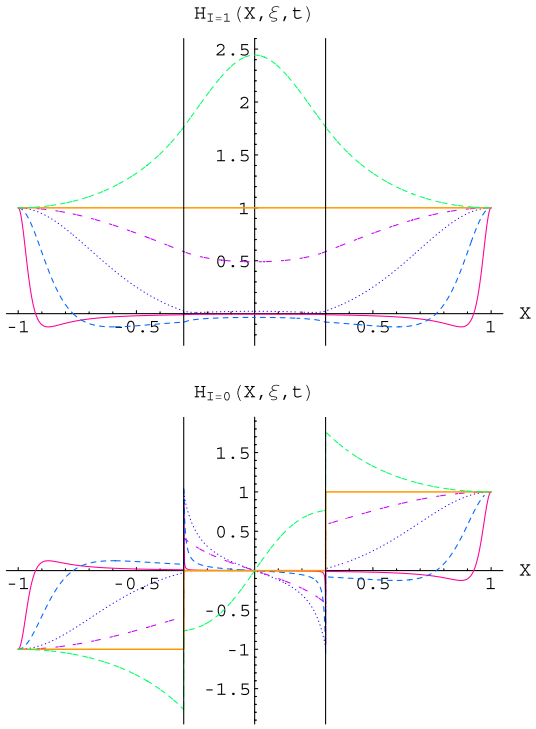

FIG. 6 (color online). Same as Fig. 5 for $H_{I=1}$ (top) and $H_{I=0}$ (bottom) in the symmetric notation, $\xi = 1/3$.

GPD's continue to be equal to 1 at $x = 1$, however very quickly drop to zero in the DGLAP region. In the ERBL region the $I = 1$ part drops, while the $I = 0$ part tends to -1 as $x \to \zeta^-$, and drops to 0 elsewhere.

Since in our quark model the parton distribution function is unity, $q(x) = 1$, the positivity bound (2.12) states that (for $t \leq 0$)

$$|H_q^{\mathrm{SQM}}(X, \xi, t)| \leq 1, \qquad \xi \leq X \leq 1. \tag{3.19}$$

It is *a priori* not obvious that the bound should hold in chiral quark models where finiteness of observables results from regularization involving subtractions. Nevertheless, we have checked with Eqs. (3.6) that condition (3.19) is actually satisfied in the DGLAP region for all values of ξ and all negative t. This is also manifest in Fig. 5, as well as in Eq. (3.18). The bound is saturated at the end points $X = \pm 1$. Thus the positivity bound is satisfied in SQM.

IV. RESULTS OF THE NAMBU–JONA-LASINIO MODEL

We use the nonlinear NJL model with Pauli-Villars (PV) regularization in the twice-subtracted version of Ref. [27]. The prescription for regularizing an observable $\mathcal{O}$ in this model is

$$\mathcal{O}_{\mathrm{reg}} = \mathcal{O}(0) - \mathcal{O}(\Lambda^2) + \Lambda^2 \frac{d\mathcal{O}(\Lambda^2)}{d\Lambda^2}, \tag{4.1}$$

where Λ is the PV regulator. Note that Eq. (4.1) is different from the prescription used in [52], where a variant of the PV regularization with two distinct cut-offs is applied. We also use the nonlinear rather than linear realization of the chiral field. In what follows we take $M = 280$ MeV for the quark mass and $\Lambda = 871$ MeV, which yields $f = 93.3$ MeV [27] according the formula

$$f^2 = -\frac{3M^2}{4\pi^2}(\log(\Lambda^2 + M^2))_{\mathrm{reg}}. \tag{4.2}$$

The pion electromagnetic form factor in the NJL model is

$$F_V^{\mathrm{NJL}}(t) = 1 + \frac{N_c M^2}{8\pi^2 f^2} \times \left(\frac{2\sqrt{4(M^2+\Lambda^2)-t}\log\left(\frac{\sqrt{4(M^2+\Lambda^2)-t}-\sqrt{-t}}{\sqrt{4(M^2+\Lambda^2)-t}+\sqrt{-t}}\right)}{\sqrt{-t}} \right)_{\mathrm{reg}}. \tag{4.3}$$

The property $\lim_{t\to-\infty} F_{\mathrm{NJL}}(t) = 0$ follows from Eq. (4.2). The isovector form factors arising in both considered models are compared in Fig. 4. The formula for the gravitational form factor in the NJL is lengthy, hence we only give the numerical results in Fig. 4. In this model also the two gravitational form factors are equal to each other, $\theta_1^{\mathrm{NJL}}(t) = \theta_2^{\mathrm{NJL}}(t)$. We note that although the form factors in both models are qualitatively similar, they are quantitatively somewhat different, which is partly due to the choice of parameters in the NJL model, as well as following from different analytic structure of the corresponding formulas, in particular, at large values of $-t$.

The application of the formulas derived in Appendix C leads to expressions similar to those of [52]. The analogs of Eq. (3.9) and (3.18) in the NJL model are more complicated, hence we do not give them here. More details may be found in Ref. [52]. For the special case of $t = 0$ Eq. (3.12) holds. As in SQM, the conditions (2.8), (2.9), and (2.10) are satisfied in the considered NJL model with the PV regularization.

The numerical results for the NJL model are displayed in Fig. 7. When comparing Figs. 6 and 7 we note a striking similarity between the two considered quark models. The slight differences stem mainly from different form factors in the two considered models, cf. Fig. 4. Our results are also qualitatively similar to the case of the chiral limit in Fig. 6 of Ref. [52]. As pointed out in Appendix C, polynomiality follows from the derivation proceeding via the double distributions. We have checked that the similarly to SQM, the positivity bound (2.12) is also satisfied in the NJL model at any ξ and all negative values of t.

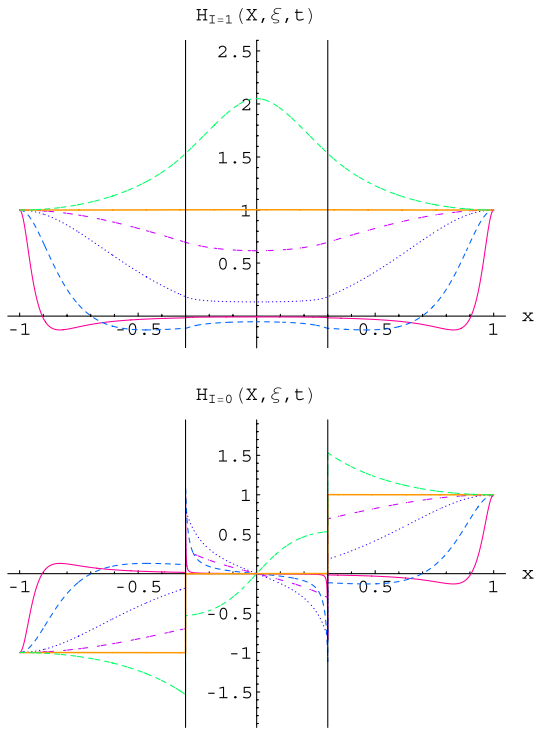

FIG. 7 (color online). Same as Fig. 6 for the NJL model with the PV regularization, $M = 280$ MeV, $\Lambda = 871$ MeV.

V. QCD EVOLUTION OF QUARK MODELS

A. The need for evolution

A key question, not only for our model but for any nonperturbative calculation, is *what* is the scale at which our model result for the GPD's holds. Ultimately, this boils down to the issue on *how* the model predictions for the GPD's might be confronted to experimental or lattice data. In QCD, the GPD's are scale dependent, while in models they correspond to functions defined at a given scale. This is so because low-energy models hold at a scale above which scaling should set in. Perturbative QCD and the corresponding scaling violations bring in the issue of evolution equations for GPD's which will be treated in detail in Sec. VI. In this section we discuss and update the procedure already used in previous works [23,27,30,31] for the evolution of PDF and PDA and extract its consequences as compared to available experimental data or lattice results.

From the point of view of perturbative QCD where both quarks and gluons contribute as *explicit* degrees of freedom, the role of the low-energy chiral quark models is to provide initial conditions for the QCD evolution equations order by order in the twist expansion. Clearly, chiral quark models contain nonperturbative QCD features, particularly the spontaneous chiral symmetry breaking. On the other hand, chiral quark models do not contain the QCD degrees of freedom, i.e., the current quarks and explicit gluons. So one expects typical high-energy perturbative QCD features, such as radiative corrections, to be absent in the model. This is precisely the pattern of logarithmic scaling violations which the models lack but which have traditionally been computed in the perturbation theory in QCD.

The procedure applied in this paper takes the quark-model distributions at some low quark-model scale Q_0 and evolves them to higher scales, where (for some observables) the experimental or lattice data are available. In the following we use the leading-order ERBL-DGLAP evolution equations with three flavors. This strategy reflects the present state of the art, which can be validated by comparing our predictions both to experiment as well as available lattice data. It should be noted, however, that to date there is no rigorous relation between the QCD quarks and the constituent quarks of the chiral models, and a more fundamental description of the transition from the hard to the soft would be very helpful.

B. Momentum fraction and the matching condition

For definiteness, we consider π^+, and denote $q(x)$ and $\bar{q}(x)$ the single-flavor distributions of quarks and antiquarks. The valence (or nonsinglet) quark distribution is

$$V = u_\pi - \bar{u}_\pi + \bar{d}_\pi - d_\pi, \tag{5.1}$$

while the nonsinglet quark distribution is

$$S = u_\pi + \bar{u}_\pi + d_\pi + \bar{d}_\pi + s_\pi + \bar{s}_\pi. \tag{5.2}$$

The sea-quark distribution is defined as

$$s = S - V = 2(\bar{u}_\pi + d_\pi) + s_\pi + \bar{s}_\pi. \tag{5.3}$$

Isospin and crossing symmetries implies the property

$$u_{\pi^+}(x) = \bar{d}_{\pi^+}(1 - x). \tag{5.4}$$

The energy-momentum tensor $\Theta^{\alpha\beta}$ is a conserved quantity in any relativistic theory and hence renormalization invariant, due to the Poincaré invariance. Its diagonal matrix element between the pion state of momentum p is

$$\langle \pi(p)|\Theta^{\alpha\beta}|\pi(p)\rangle = 2p^\alpha p^\beta. \tag{5.5}$$

For the QCD Lagrangian the energy-momentum tensor can be separated into several contributions in a gauge-invariant but scale- and hence scheme-dependent manner [60]. Although we will be considering the LO evolution, for our purposes we may have the standard $\overline{\text{MS}}$ scheme in mind and write

$$\Theta^{\alpha\beta} = \Theta_g^{\alpha\beta} + \Theta_s^{\alpha\beta} + \Theta_v^{\alpha\beta} \tag{5.6}$$

where $\Theta_g^{\alpha\beta}$, Θ_s, and $\Theta_v^{\alpha\beta}$ are the gluon, sea-quark, and valence-quark contributions, respectively. They are equal to

$$\langle\pi|\Theta_g^{\alpha\beta}|\pi\rangle|_\mu = 2p^\alpha p^\beta\langle x\rangle_g(\mu),$$
$$\langle\pi|\Theta_s^{\alpha\beta}|\pi\rangle|_\mu = 2p^\alpha p^\beta\langle x\rangle_s(\mu), \quad (5.7)$$
$$\langle\pi|\Theta_v^{\alpha\beta}|\pi\rangle|_\mu = 2p^\alpha p^\beta\langle x\rangle_v(\mu)$$

where $\langle x\rangle_g(\mu)$, $\langle x\rangle_s(\mu)$, and $\langle x\rangle_v(\mu)$, are the gluon, sea-quark, and valence-quark *momentum fractions* of the pion at the scale μ, respectively. In deep inelastic scattering (DIS) it can be shown [61] that if $q(x,\mu)$, $\bar{q}(x,\mu)$, and $G(x,\mu)$ represent the probability density of finding a quark, antiquark, and gluon, respectively, with the momentum fraction x at the scale μ (typically, we identify μ^2 with Q^2 in DIS), then

$$\langle x\rangle_g(\mu) = \int_0^1 dx x G(x,\mu), \quad (5.8)$$

$$\langle x\rangle_s(\mu) = \int_0^1 dx x s(x,\mu), \quad (5.9)$$

$$\langle x\rangle_v(\mu) = \int_0^1 dx x V(x,\mu), \quad (5.10)$$

where, due to the crossing symmetry (5.4) for a single flavor one has $\langle x\rangle_q = \langle x\rangle_u = \langle x\rangle_{\bar{d}} = \langle x\rangle_v/2$. The scale-dependent momentum fractions fulfill the momentum sum rule

$$\langle x\rangle_g(\mu) + \langle x\rangle_s(\mu) + \langle x\rangle_v(\mu) = 1, \quad (5.11)$$

which is a consequence of the energy-momentum tensor conservation. In perturbation theory due to radiative corrections $\langle x\rangle_g(\mu)$ and $\langle x\rangle_s(\mu)$ decrease as the scale μ goes down. On the contrary, the valence contribution to the energy-momentum tensor evolves as

$$\frac{\langle x\rangle_v(Q)}{\langle x\rangle_v(Q_0)} = \left(\frac{\alpha(Q)}{\alpha(Q_0)}\right)^{\gamma_1^{(0)}/(2\beta_0)}, \quad (5.12)$$

where $\gamma_1^{(0)}/(2\beta_0) = 32/81$ for $N_F = N_c = 3$. Downward LO QCD evolution would yield that for some given reference scale, $\mu_0 \equiv Q_0$,

$$\langle x\rangle_v(Q_0) = 1, \qquad \langle x\rangle_s(Q_0) + \langle x\rangle_g(Q_0) = 0. \quad (5.13)$$

The scale Q_0 defined with the above condition is called the *quark-model scale* for obvious reasons, as only valence quarks contribute. This may represent the matching condition between QCD and the chiral quark models, schematically written as Eq. (1.6).

There exists a wealth of information on the momentum fraction carried by valence quarks in the pion at scales $Q \sim 2$ GeV, coming from several sources. Phenomenological analyses require these high scales to neglect higher-twist corrections. The Durham group [62], based mainly on the E615 Drell-Yan data [53] and the model assumption that sea quarks carry 10–20% of the momentum fraction, determines $\langle x\rangle_q = 0.235(10)$ at the scale $Q = 2$ GeV. The analysis of Ref. [63], based on the assumption that the momentum fraction carried by valence quarks in the pion coincides with that of the nucleon, yields $\langle x\rangle_q = 0.2$ at $Q = 2$ GeV.

Other determinations, comprising lattice calculations, may access directly the leading-twist contribution in a nonperturbative manner. However, the transition from the intrinsically nonperturbative lattice regularization to the perturbative $\overline{\rm MS}$ regularization scheme requires high-energy matching scales. Early Euclidean lattice simulations provided $\langle x\rangle_q = 0.32(5)$ at the scale $Q^2 \approx 4.84 \pm 2.2$ GeV^2 [64]. More recently, lattice calculations linearly extrapolated to the chiral limit [65], yielding $\langle x\rangle_q = 0.28(1)$ at the scale $Q^2 \approx 5.8$ GeV^2, a somewhat larger value than suggested by phenomenology [62,63] and expected from the quenched approximation. Still, in the quenched approximation, in Ref. [66] $\langle x\rangle_q = 0.243(21)$ at $Q = 2$ GeV for light pions, which is in a closer agreement to the Durham [62] than to the Dortmund [63] results. This value squares with the gluon content of the pion $\langle x\rangle_g = 0.37 \pm 0.08_{\rm stat} \pm 0.12_{\rm sys}$ at a similar scale but with $m_\pi \sim 900$ MeV, as extracted recently in Ref. [67].

Finally, there exist transverse lattice calculations, where full x-dependent parton properties can be determined nonperturbatively at low scales [12]. The calculation of Ref. [68] gives $\langle x\rangle_q = 0.43(1)$ at $Q^2 \sim 1$ GeV^2, whereas Ref. [69] provides, still at very low scales $Q^2 \sim 0.4$ GeV^2, the value $\langle x\rangle_q \approx 0.38$.

For definiteness we adopt the values used in previous works [23,27,30,31], namely, that at $Q^2 = 4$ GeV^2 the valence quarks carry 47% of the total momentum in the pion [62,66], e.g., for π^+,

$$\langle x\rangle_v = 0.47(2), \quad (5.14)$$

at $Q^2 = 4$ GeV^2. At LO the scale turns out to be

$$Q_0 = 313^{+20}_{-10}\ \text{MeV}, \quad (5.15)$$

where the value of $\Lambda_{\rm QCD}$ is provided in Eq. (1.5) and the error reflects the uncertainty in Eq. (5.14). At such low scale the perturbative expansion parameter in the evolution equations is large, $\alpha(Q_0^2)/(2\pi) = 0.34$, which makes the evolution very fast for the scales close to the initial value. We return to this issue below.

C. Evolution of PDF

In Fig. 8 we display the forward diagonal PDF of the pion, in particular, the quantity $xq(x) = xH_q^{I=1}(x,0,0)$ obtained with the LO QCD evolution up to $Q = 4$ GeV from the quark-model initial condition, $q(x,Q_0) = 1$ [23]. At leading order the standard DGLAP evolution holds, which for the Mellin moments reads

$$\int_0^1 dx x^n q(x,Q) = \frac{1}{n+1}\left(\frac{\alpha(Q)}{\alpha(Q_0)}\right)^{\gamma_n^{(0)}/(2\beta_0)}, \quad (5.16)$$

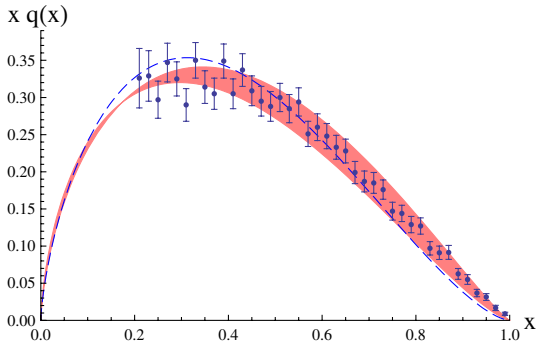

FIG. 8 (color online). The quark-model prediction for the valence PDF of the pion for a single quark (either u or $\bar{d}$ for π^+) evolved to the scale of $Q = 4$ GeV (band). The width of the band indicates the uncertainty in the initial scale Q_0, Eq. (5.15). The data points come from the analysis of the Drell-Yan data from the E615 experiment [53]. The dashed line shows the recent reanalysis of the original data made in Ref. [70].

where the anomalous dimensions for the vector vertex are given by

$$\gamma_n^{(0)} = -2C_F\left[3 + \frac{2}{(n+1)(n+2)} - 4\sum_{k=1}^{n+1}\frac{1}{k}\right], \quad (5.17)$$

with $C_F = (N_c^2 - 1)/(2N_c)$. The evolution equations can be solved via the inverse Mellin transformation. In Fig. 8 we confront the result for $xq(x, Q)$ at the scale $Q = 2$ GeV with the data at the same scale from the E615 Drell-Yan experiment [53]. The model results are represented with a band, which reflects the uncertainty in the determination of the scale Q_0 in Eq. (5.15). The quality of this comparison is impressive, which shows that despite the rather embarrassingly low value of the scale Q_0, the quark-model initial condition leads to fair phenomenology. The next-to-leading order (NLO) evolution leads to small changes as compared to the LO results [30], in fact compatible with the experimental uncertainties. The dashed line represents the recent reanalysis of the original E615 data made in Ref. [70]. We note that this result is also close to the band generated by our quark-model calculations.

Moments of PDF's have been calculated on Euclidean lattices [65], yielding $\langle x\rangle_v = 0.3(1)$, $\langle x^2\rangle_v = 0.10(5)$, and $\langle x^3\rangle_v = 0.05(1)$ at $Q = 2.4$ GeV. In Ref. [66] $\langle x\rangle_v = 0.243(21)$ at $Q = 2$ GeV.

The nonsinglet PDF in the pion was also evaluated on the transverse lattice [71] at the low renormalization scale $Q \sim 0.5$ GeV. In Fig. 9 we show our PDF evolved to that scale (darker band) and to a lower scale of 0.35 GeV (lighter band). We take the liberty of moving the scale, as its determination on the lattice is not very precise. As we see, the agreement is qualitatively good if one considers the uncertainties of the data, especially when the lower scale is used. We also show the GRV98 parametrization [72] (dashed line), which gives somewhat lower PDF (except low values of x) compared to the lattice data and our model results.

D. Evolution of PDA

PDA's have been intensely studied in the past in several contexts (see, e.g., [73–76] and Ref. [77] for a brief but comprehensive review). The PDA of the pion [31], which can be related to the isovector GPD through the soft-pion theorem, Eq. (2.18), is $\phi(x; Q_0) = 1$, which holds at the quark-model scale Q_0 (5.15) [31]. The evolved PDA can be expressed in terms of the Gegenbauer polynomials [78,79]

$$\phi(x, Q) = 6x(1-x)\sum_{n=0}^{\infty\prime} C_n^{3/2}(2x-1)a_n(Q), \quad (5.18)$$

where the prime indicates summation over even values of n only. Our initial condition yields [31]

$$a_n(Q) = \frac{2}{3}\frac{2n+3}{(n+1)(n+2)}\left(\frac{\alpha(Q)}{\alpha(Q_0)}\right)^{\gamma_n^{(0)}/(2\beta_0)}, \quad (5.19)$$

where the anomalous dimension for the axial-vector vertex is the same as for the vector vertex, $\gamma_n^{(0)}$, given in Eq. (5.17). The evolved PDA is shown in Fig. 10, where it is compared to the E791 di-jet measurement [54]. The normalization of the di-jet data is used as a fit parameter. Besides this normalization the result is *parameter free*. As we see the agreement with the E791 data is rather reasonable with a $\chi^2/\mathrm{DOF} = 1.45$. Nonetheless, the asymptotic wave function generates a yet better $\chi^2/\mathrm{DOF} = 0.45$. Note that in our scheme such a extreme limit would correspond to taking $Q_0 = \Lambda_{\mathrm{QCD}}$.

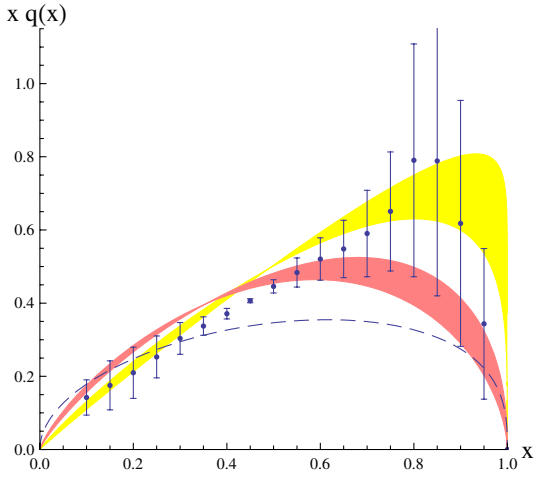

FIG. 9 (color online). The quark-model prediction for the valence PDF of the pion for a single quark (either u or $\bar{d}$ for π^+) evolved to the scale $Q = 0.5$ GeV (darker band) and $Q = 0.35$ GeV (lighter band). The width of the bands indicates the uncertainty in the initial scale Q_0, Eq. (5.15). The data come from the transverse lattice calculations [71] and correspond to the scale ~0.5 GeV. The line shows the Gluck-Reya-Schienbein [72] parametrization at $Q = 0.5$ GeV.

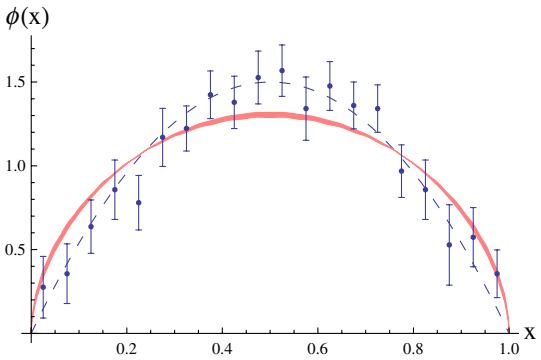

FIG. 10 (color online). The quark-model prediction for the PDA evolved to the scale $Q = 2$GeV (band) and compared to the E791 di-jet measurement [54] after proper normalization of the data. The width of the band indicates the uncertainty in the initial scale Q_0, Eq. (5.15). We also show the asymptotic PDA, $\phi(x, \infty) = 6x(1 - x)$ (dashed line).

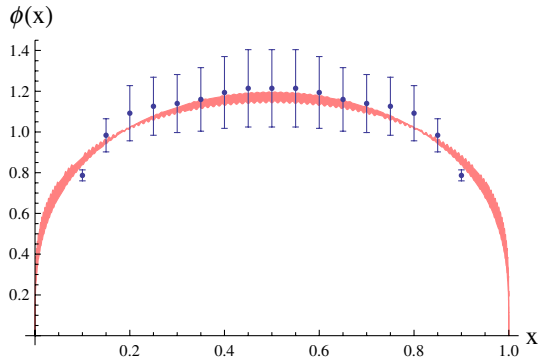

FIG. 11 (color online). The quark-model prediction for PDA evolved to the scale $Q = 0.5$ GeV (band) compared to the transverse lattice data [71], corresponding to the scale ~0.5 GeV. The width of the band corresponds to the uncertainty in the initial scale Q_0, Eq. (5.15).

The second Gegenbauer moment at the scale $Q = 2.4$ GeV is $a_2 = 0.12$ to be compared with the value $a_2 = 0.12(3)$ based on the analysis of the CLEO data of Ref. [80] where it was assumed that $a_n = 0$ for $n > 4$.

Further, the leading-twist contribution to the pion transition form factor is, at the LO in the QCD evolution [78], equal to

$$\frac{Q^2 F_{\gamma^*\to\pi\gamma}(Q)}{2f}\bigg|_{\text{twist}-2} = \int_0^1 dx \frac{\phi(x, Q)}{6x(1-x)}. \tag{5.20}$$

The experimental value obtained in CLEO [81] for the full form factor is $Q^2 F_{\gamma^*,\pi\gamma}(Q)/(2f) = 0.83 \pm 0.12$ at $Q^2 = (2.4\ \text{GeV})^2$. Our value for the integral, 1.25 ± 0.10, overestimates the experimental result by about 2 standard deviations, but one should bare in mind that higher-twist contributions as well as NLO perturbative corrections have been ignored.

The second ξ-moment ($\xi = 2x - 1$), defined as

$$\langle \xi^2 \rangle_Q = \int_0^1 dx \phi(x, Q)(2x - 1)^2, \tag{5.21}$$

has been computed on Euclidean lattices yielding $\langle \xi^2 \rangle = 0.286(49)$ [82], $\langle \xi^2 \rangle = 0.269(39)$ [83], $\langle \xi^2 \rangle = 0.278(26)$ [84] from recent Euclidean lattice calculations at the scale $Q = 1/a \sim 2.6 \pm 0.1$ GeV, where a is the lattice spacing. Note that the asymptotic PDA would yield $\langle \xi^2 \rangle = 1/5 = 0.20$. We get from the quark model $\langle \xi^2 \rangle = 0.244(4)$ for that scale.

In Fig. 11 we compare our model prediction for the PDA (band) to the transverse lattice data [71] at the scale $Q = 0.5$ GeV. A good agreement is observed.

One of the most surprising aspects is that many of these results can be obtained from the integral relation between PDF's and PDA's at a given scale, established in Ref. [31]. The relation allows one to *predict* $\phi(x, Q)$ from $V(x, Q)$ as parametrized, e.g., by the Durham group [62]. The method works for quark models, where $V(x, Q_0) = \phi(x, Q_0) = 1$ at some scale Q_0.

E. End-point behavior

The results at the quark-model scale exhibit discontinuity at $x = 0, 1$, as $V(x, Q_0) = \phi(x, Q_0) = 1$. An important feature of the evolution is that it cures the end-point behavior of the PDF's and PDA's [27,31,85]. Using the Mellin-moments formulation of the LO DGLAP evolution it can be shown that if $V(x, Q_0) \sim c(1 - x)^p$ near $x = 1$ then

$$V(x, Q) \sim c(1 - x)^{p + 8r(Q_0, Q)}, \qquad x \to 1, \tag{5.22}$$

where we have introduced the short-hand notation

$$r(Q_0, Q) = \frac{C_F}{2\beta_0} \log \frac{\alpha(Q_0)}{\alpha(Q)} \tag{5.23}$$

and c and p are some constants. Specifically, in our quark-model case $c = 1$ and $p = 0$. The prefactor can also be obtained, yielding the more accurate formula [85]

$$V(x, Q) \sim \frac{e^{2(3-4\gamma)r(Q_0,Q)}}{\Gamma(1 + 8r(Q_0, Q))}(1 - x)^{8r(Q_0,Q)}, \tag{5.24}$$

where $x \to 1$, γ denotes the Euler-Mascheroni constant, and Γ is the Euler gamma function. At $Q > 1$ GeV the exponent of $1 - x$ is a function weakly dependent on Q. The explicit forms for several values of Q and Q_0 from Eq. (5.15) are

$$\begin{aligned} V(x, 0.5\ \text{GeV}) &\sim 1.23(1 - x)^{0.53}, \\ V(x, 2.4\ \text{GeV}) &\sim 1.13(1 - x)^{1.17}, \\ V(x, 10\ \text{GeV}) &\sim 1.00(1 - x)^{1.45}. \end{aligned} \tag{5.25}$$

These are compared to the full result in the left panel of Fig. 12.

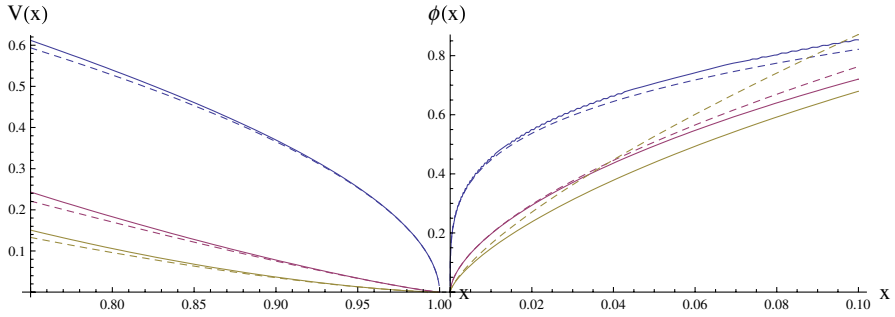

FIG. 12 (color online). Comparison of the full result of the QCD evolution (solid lines) to the asymptotic formulas near the end points (dashed lines). Left—valence PDF, right—PDA. The curves from top to bottom are for $Q = 0.5$, 2.4, and 10 GeV, respectively. The initial scale Q_0 is taken from Eq. (5.15).

Similarly, for the PDA evolved with the help of the Gegenbauer polynomials (see Appendix E for the derivation), one can show that[5]

$$\phi(x, Q) \sim -\frac{\Gamma(-4r(Q_0, Q))}{\Gamma(4r(Q_0, Q))} e^{2(3-4\gamma)r(Q_0,Q)} x^{4r(Q_0,Q)}, \quad x \to 0, \tag{5.26}$$

and a symmetric expression when $x \to 1$ with x replaced by $1 - x$. With several explicit values for Q we have

$$\begin{aligned} \phi(x, 0.5\ \text{GeV}) &\sim 1.51 x^{0.26}, \\ \phi(x, 2.4\ \text{GeV}) &\sim 2.95 x^{0.59}, \\ \phi(x, 10\ \text{GeV}) &\sim 4.65 x^{0.73}, \end{aligned} \tag{5.27}$$

all for Q_0 from Eq. (5.15). These asymptotic forms are compared to the full result of the QCD evolution in the right panel of Fig. 12. We note that the range of validity of the approximation (5.26) shrinks closer and closer to the end point as Q is increased. This must be so, as at $Q \to \infty$ the asymptotic form $6x(1 - x)$ sets in the whole range of x, while the power $r(Q_0, Q)$ increases indefinitely with Q.

It should be noted that the behavior of Eqs. (5.22),(5.26), exhibiting the desired continuity of the functions at the end points, is achieved already at values of Q *infinitesimally* larger than Q_0. Thus the QCD evolution heals the end-point problem immediately, at any $Q > Q_0$. Such a phenomenon is linked to the nonuniform convergence of the Mellin or Gegenbauer functional series near the end points for the PDF and PDA, respectively.

F. Evolution of diagonal GPD in the impact-parameter space

The impact-parameter dependence quoted in Eq. (3.14) at the quark-model point [32] not only satisfies the model-independent relation (2.15) but after proper smearing over plaquettes and DGLAP evolution qualitatively reproduces both the Bjorken x and impact-parameter dependence when compared to transverse lattice results [86,87] at the rather low scale $Q \sim 0.5$ GeV. This is a remarkable finding, since the transverse lattice at such low scales should incorporate nonperturbative evolution effects if they happened to be important. Details can be found in Ref. [32].

G. Discussion

To summarize this section, the low value of the renormalization scale Q_0 deduced from the LO perturbative evolution of the momentum fraction complies surprisingly well with a wealth of fragmentary information for the nonsinglet partonic distributions both on the experimental side as well as compared to Euclidean lattices at $Q \sim 2$ GeV and transverse lattices at $Q \sim 0.5$ GeV. This provides some confidence on applying a similar strategy to the evolution of nonsinglet GPD's as we do in the next section. Of course, it would be of great help to have Euclidean lattices at small renormalization scales, such that some of the nonperturbative evolution could be explicitly seen. Unfortunately, the transition from the intrinsically nonperturbative lattice regularization to the perturbative $\overline{\text{MS}}$ regularization scheme requires high scales, so such a calculation seems hardly viable. Transverse lattices do not suffer from this drawback, as these are nonperturbative calculations at low scales [12]. We are in qualitative agreement also with these lattice calculations, which probe the evolution in a region where it might potentially be highly nonperturbative. Our analysis agrees within uncertainties with a picture where the main nonperturbative feature of the valence-quark contribution is provided by the initial condition. In any case, as shown in the LO and NLO analysis of Ref. [30], the sea-quark and gluon PDF's from chiral quark models are less properly reproduced. This might be improved if some nonsinglet, either sea or gluonic model, contributions could be provided at the model scale, Q_0. Despite the efforts all over the years the problem of determining the nonperturbative gluon content in a hadron at low scales has remained unresolved. These provisos should be taken in mind when evolving the singlet GPD's in our scenario.

[5]The corresponding formula in Ref. [31] has a mistake.

VI. THE QCD EVOLUTION OF GPD'S

The explicit form of the LO QCD evolution equations for the GPD's can be found in [88–94]. In this paper we solve them with the numerical method developed in [92], based on the Chebyshev polynomial expansion.

As extensively discussed in the previous section, perturbative QCD brings in the issue of evolution equations for the GPD's. Similarly to the more familiar case of the PDF, the QCD interactions of massless partons lead to collinear divergences which are factored out and absorbed into the GPD's. As a result, the GPD's become dependent on a factorization (renormalization) scale μ, usually identified with the hard scale, $\mu = Q$. Thus, in general, the GPD's are functions of four variables, $H = H(X, \xi, t, Q^2)$, with the kinematic constraints $|X| \leq 1$ and $0 \leq \xi \leq 1$. The renormalization group equations which govern the dependence of GPD's on Q^2 are described in detail, e.g., in Ref. [92]. The form of these equations depends on the asymmetry parameter ξ, which defines two regions: the ERBL region for $|X| \leq \xi$, and the DGLAP region for $|X| \geq \xi$.

An important feature of the GPD evolution, which makes it more complicated than in the case of PDF or PDA, is that the evolution equations in the ERBL region depend on the values of GPD's in the DGLAP region. The converse is not true, the evolution in the DGLAP region is not influenced by the ERBL region.

Asymptotically, for $Q^2 \to \infty$, the GPD's tend to the asymptotic forms which are concentrated in the ERBL region only. In particular, for $|X| < \xi$ we have

$$
\begin{aligned}
H^{I=1} &= \frac{3}{2\xi}\left(1 - \frac{X^2}{\xi^2}\right)F_V(t), \\
H^{I=0} &= (1-\xi^2)\frac{15}{4\xi^2}\frac{N_f}{4C_F + N_f}\frac{X}{\xi}\left(1 - \frac{X^2}{\xi^2}\right)\theta(t), \\
XH_g &= (1-\xi^2)\frac{15}{16\xi}\frac{4C_F}{4C_F + N_f}\left(1 - \frac{X^2}{\xi^2}\right)^2\theta(t)
\end{aligned}
\tag{6.1}
$$

while the GPD's vanish for $|X| \geq \xi$. The proportionality constants reflect the normalization of the GPD's at the initial scale Q_0, as the following charge- and momentum-conservation sum rules are preserved by the evolution

$$
\begin{aligned}
&\int_{-1}^{1} dX H^{I=1}(X, \xi, t, Q^2) = 2F_V(t), \\
&\int_{-1}^{1} dX (XH^{I=0}(X, \xi, t, Q^2) \\
&\qquad + XH_g(X, \xi, t, Q^2)) = (1-\xi^2)F_S(t),
\end{aligned}
\tag{6.2}
$$

in accordance to Eq. (2.9) and (2.10).

The results of the LO evolution from the SQM initial condition at the scale Q_0 up to $Q = 4$ GeV and $\xi = 1/3$ are shown in Fig. 13. In each of the four sets of plots, corresponding to a different value of t, we show the quark nonsinglet $H^{I=1}$ (top) and singlet (middle) $H^{I=0}$ distributions together with the gluon H_g (bottom), conventionally multiplied by X. We have chosen the sample value $\xi = 1/3$, since the results are qualitatively similar for other values of ξ. The solid lines show the initial condition at the quark-model scale Q_0 of Eq. (5.15), the dashed lines show the result of the LO QCD evolution to the scale $Q = 4$ GeV, and the dotted lines show the asymptotic forms at $Q \to \infty$ given in Eq. (6.1). As the value of $-t$ is increased, the magnitudes of the curves becomes lower, conforming to the sum rules (2.9),(2.10). We note that the evolution smooths out the original distributions, in particular, the discontinuities at the end points, $X = \pm 1$, and at the ERBL-DGLAP matching points $X = \pm\xi$ disappear for the isosinglet GPD.

The results for the NJL model are very similar to the case of SQM. In Fig. 14 we show them for $t = -1$ GeV^2 and $\xi = 1/3$. This similarity between the models is a sheer reflection of the numerical similarity in the initial condition, cf. Fig. 13 for $t = -1$ GeV^2 and Fig. 14.

In Fig. 15 it is shown how slow the evolution is in reaching the asymptotic forms of the GPD's. The evolution is fastest at low values of Q, where the coupling constant is large, and it immediately pulls down the end-point values to zero. Then, the strength gradually drifts from the DGLAP regions to the ERBL region. Yet, the approach to the asymptotic form is very slow, with the tails in the DGLAP region present. The highest Q^2 displayed in the figure is 10^8 GeV^2 and the asymptotic form is reached at "cosmologically" large values of Q, which are never achieved experimentally. Thus, the only way to approach the asymptotics would be to start from initial conditions which are already close to it. We also observe that at larger $-t$ more strength of the quark GPDs resides in the DGLAP region. This feature reflects the shape of the initial condition, which inhibits the strength in the ERBL region. Evolution up to $Q = 2$ GeV retains this behavior, which gradually disappears as $Q \to \infty$ where all the strength settles in the ERBL region.

We note that the desired vanishing of the GPD's at the end points $X = \pm 1$ is achieved due to the QCD evolution, similarly to the results presented in Sec. V E. Also, evolution leads to continuity at the DGLAP-ERBL boundary, $X = \pm\xi$. These features are achieved at scales Q infinitesimally above Q_0.

VII. CONCLUSIONS

We summarize our main points. In the present paper we have dealt with the determination of the leading-twist GPD's of the pion in field-theoretic chiral quark models. We have done so with the help of an efficient method using the α-representation of the quark propagators and an extensive use of double distributions. Our calculation incorporates the necessary D-terms required by polynomiality and dimensional analysis. In the chiral limit, we have been able to determine explicit analytic formulas for the pion

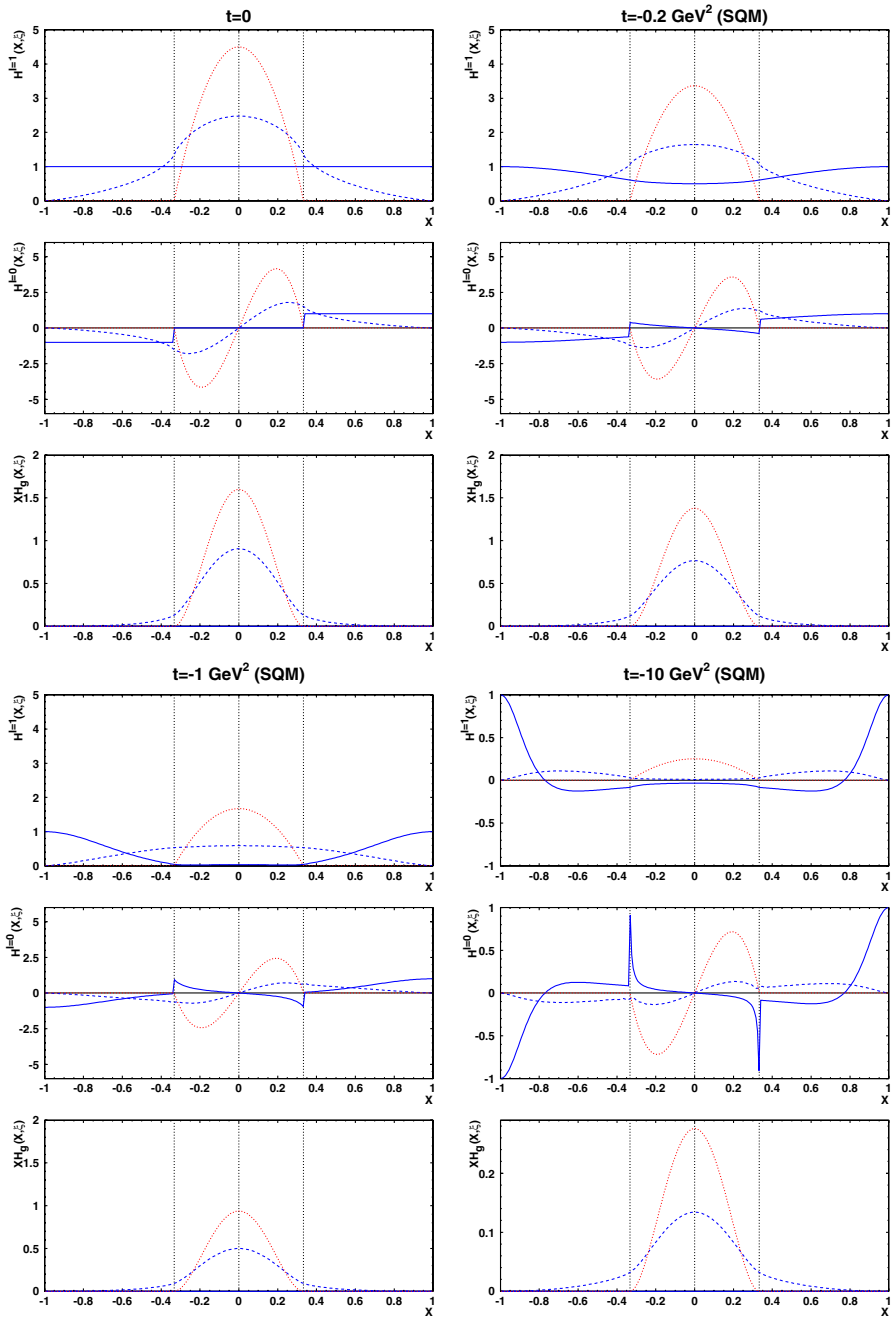

FIG. 13 (color online). Results of the LO QCD evolution from the SQM initial condition for several values of t and $\xi = 1/3$. Solid lines—initial condition at the quark-model scale, dashed lines—evolution to $Q^2 = (4\ \mathrm{GeV})^2$, dotted lines—asymptotic form, $Q^2 \to \infty$.

GPD's. All *a priori* properties which ought to be satisfied on general principles, namely, polynomiality, positivity, proper support, soft-pion theorems, sum rules, and normalization are indeed fulfilled explicitly by our model calculation. Although one might superficially think that these properties should be trivially satisfied, the fact that one deals with regularization or momentum dependence makes the fulfillment of those properties less obvious, and in fact many calculations violate some property. A key ingredient in our approach has been a scrupulous treatment of regularization in conjunction with electromagnetic and chiral Ward-Takahashi identities. Our results for the pionic GPD's in the NJL model agree with Ref. [52].

In the two chiral quark models considered, NJL and SQM, we have found results looking alike since the models are mainly fixed by the pion charge form factor which in both cases looks very similar. In addition, we have determined the pion gravitational form factor entering the momentum-conservation sum rule. The outcoming GPD's are not t-factorizable, an assumption which is being

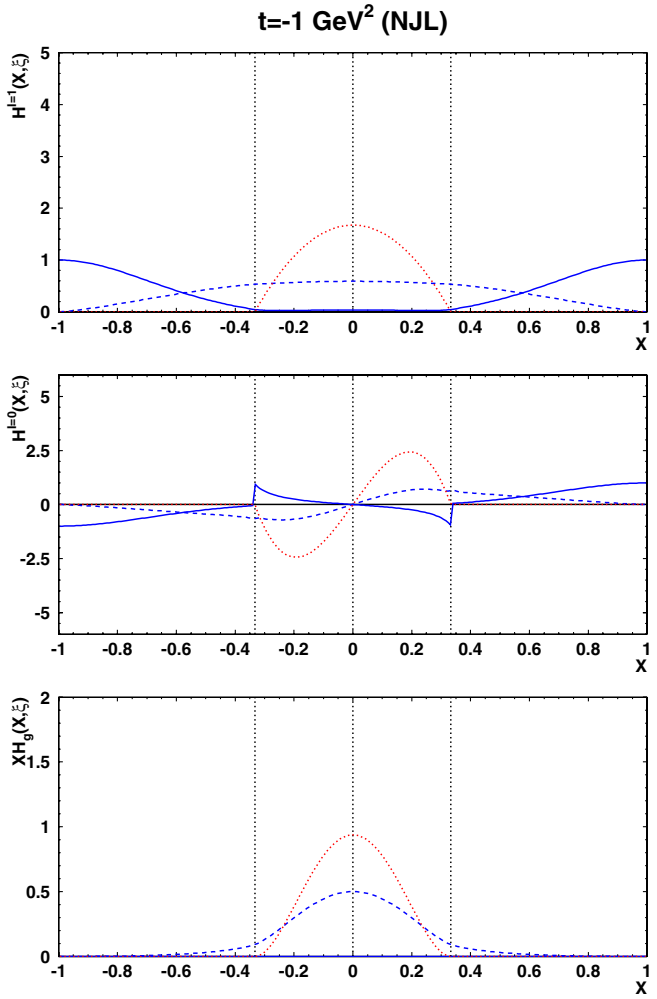

FIG. 14 (color online). Same as bottom left panel of Fig. 13 for the NJL model.

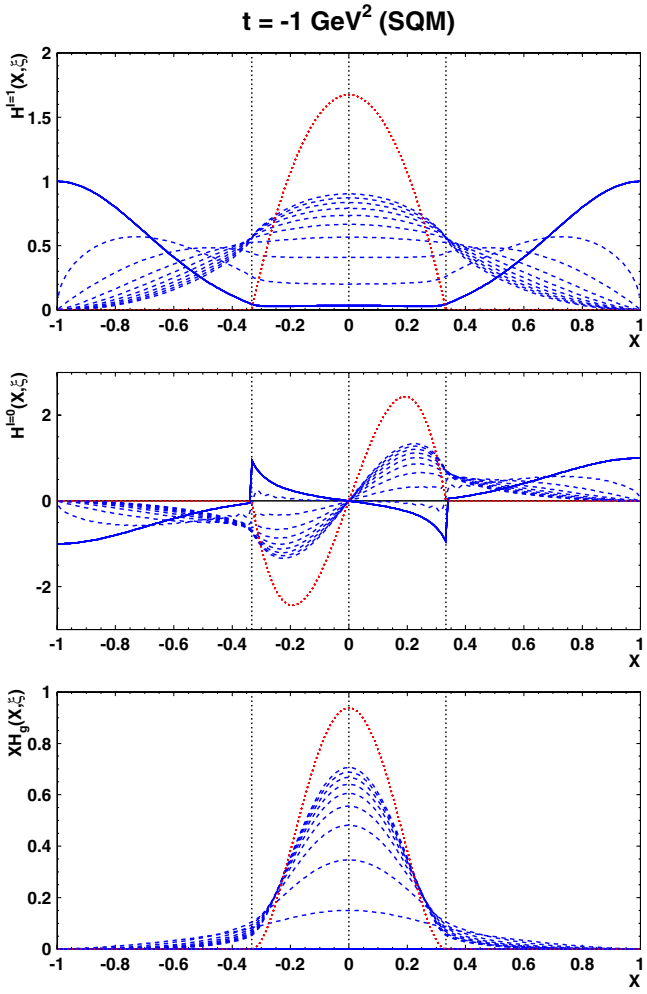

FIG. 15 (color online). Same as Fig. 13 for subsequent evolution scales: $Q^2 = 0.1, 1, 10, 10^2, \ldots, 10^8$ GeV^2. Higher Q^2 gives higher magnitude of the curves in the ERBL region.

extensively used in phenomenological approaches, not based on consistent dynamical calculations.

However, with all those desirable properties fulfilled, one must undertake the ERBL-DGLAP QCD evolution in order to relate the model results to experimental high-energy data where higher-twist contributions to the GPD's can be disregarded. Likewise, a comparison to lattice results of the twist-2 GPD's requires specification of a running scale. This aspect of the calculation is most frequently ignored in dynamical model calculations, and particularly in chiral quark models. A practical comparison to either experiment or lattice can be achieved by matching the momentum fraction of the QCD evolved quark model to the experimental or lattice-extracted result. In practice, the LO perturbative evolution is used with the result that the low-energy quark-model scale is very low. Nevertheless, once this is fixed the GPD's are uniquely determined. We have confronted our predictions with all available information extracted either from experiment or lattice both transverse or Euclidean. The experimental data include the Fermilab E615 and E791 measurements of PDF and PDA of the pion, respectively, and CLEO measurements on the pion transition form factor. The reasonable overall agreement to all these data corresponding to quite different kinematical situations should be stressed. This fact provides some confidence on our predictions of the nonsinglet leading-twist GPD's. This also applies to the pion-photon transition distribution amplitude, determined recently in quark models [35].

ACKNOWLEDGMENTS

Supported by Polish Ministry of Science and Higher Education, Grants No. 2P03B 02828 and No. N202 034 32/0918, Spanish DGI and FEDER funds with Grant No. FIS2005-00810, Junta de Andalucía Grant No. FQM225-05, and EU Integrated Infrastructure Initiative Hadron Physics Project Contract No. RII3-CT-2004-506078. We warmly thank Sasha Bakulev and Simon Dalley for providing us with the experimental and transverse lattice data, respectively.

APPENDIX A: THE α-REPRESENTATION EVALUATION OF THE TWO- AND THREE-POINT FUNCTIONS

In studies based on quark models the simplest way to obtain the GPD's and the double distributions is through the use of the α-representation for the scalar propagators. The advantage of this representation over other popular Feynman parametrizations of one-loop functions relies in the fact that the $\delta(k\cdot n - x)$ function constraining the loop integration is also naturally written in terms of an integral of an exponential. This allows for maintaining the explicit Lorentz covariance throughout the calculation. In our scheme one does not have to start with the somewhat cumbersome moments in $k\cdot n$, and then "invert" the result, as is frequently done. The method used in this paper leads to well-defined and very simple algebra and reproduces the double distributions in chiral quark models from the literature. Also, in our approach the otherwise subtle effect of the emergence of the D-terms follows in a clear way just from the Feynman diagrams.

Below we derive basic integrals appearing later on in the evaluation of the GPD's. Calculations of this appendix are made in the Euclidean space. We denote the Euclidean scalar propagators of particles of mass ω as

$$S_k = \frac{1}{D_k} = \frac{1}{k^2+\omega^2} = \int_0^\infty d\alpha e^{-\alpha(k^2+\omega^2)}, \tag{A1}$$

where the right-hand side displays the α-representation.

1. Two-point functions

Let us first consider the function $I(x, l\cdot n, 0, l^2)$ corresponding to the definition (2.26) with the choice $l' = 0$. This two-point function with the constrained $k\cdot n$ integration can be written as

$$\begin{aligned} I(x,\kappa,0,l^2) &= \frac{4N_c\omega^2}{f^2}\int\frac{d^4k}{(2\pi)^4}\delta(k\cdot n - x)S_kS_{k-l} \\ &= \frac{4N_c\omega^2}{f^2}\int\frac{d^4k}{(2\pi)^4}\int\frac{d\lambda}{2\pi}e^{i\lambda(k\cdot n-x)}\int_0^\infty da\int_0^\infty db e^{-a(k^2+\omega^2)-b((k-l)^2+\omega^2)} \\ &= \frac{4N_c\omega^2}{f^2}\int\frac{d^4k'}{(2\pi)^4}\int_0^\infty da\int_0^\infty db\int\frac{d\lambda'}{2\pi}(a+b)e^{-(a+b)(k'^2+\omega^2)-(ab/a+b)l^2+i\lambda'(b\kappa-(a+b)x)} \\ &= \frac{4N_c\omega^2}{f^2}\int\frac{d^4k'}{(2\pi)^4}\int_0^\infty da\int_0^\infty db\delta[b\kappa-(a+b)x](a+b)e^{-(a+b)(k'^2+\omega^2)-(ab/a+b)l^2}, \end{aligned} \tag{A2}$$

where for brevity $\kappa = n\cdot l$, the shifted integration momentum is $k' = k + \frac{b}{a+b}l + \frac{i}{2}\lambda' n$, and $\lambda' = \lambda/(a+b)$. The $\delta[b\kappa-(a+b)x]$ function gives the constraint

$$x = \frac{b\kappa}{a+b}. \tag{A3}$$

Since the integration variables are positive, $a, b \geq 0$, it follows immediately that $x\in[0,\kappa]$ for $\kappa\geq 0$ and $x\in[-\kappa,0)$ for $\kappa<0$. This provides the proper support for $I(x,\kappa,0,l^2)$, which can be written generally as $\theta[x(\kappa-x)]$.

One can decompose the k' integration into two parts,

$$dk'^0dk'^3 = \pi dK^2, \qquad dk'^1dk'^2 = \pi du, \tag{A4}$$

with $K^2 = (k'^0)^2 + (k'^3)^2$ and the "transverse" momentum $u = (k'^1)^2 + (k'^2)^2$. Then

$$\begin{aligned} I(x,\kappa,0,l^2) &= \frac{N_c\omega^2\theta[x(\kappa-x)]}{4\pi^2f^2}\int_0^\infty du\int_0^\infty da\int_0^\infty db\delta[b\kappa-(a+b)x]e^{-(a+b)(u+\omega^2)-(ab/a+b)l^2} \\ &= \frac{N_c\omega^2\theta[x(\kappa-x)]}{4\pi^2f^2|\kappa|}\int_0^\infty du\int_0^\infty db' e^{-b'[u+\omega^2+(x/\kappa)(1-(x/\kappa))]} \\ &= \frac{N_c\omega^2\theta[x(\kappa-x)]}{4\pi^2f^2|\kappa|}\int_0^\infty du\frac{1}{u+\omega^2+\frac{x}{\kappa}(1-\frac{x}{\kappa})l^2}, \end{aligned} \tag{A5}$$

where $b' = b\kappa/x$. The integral over u is logarithmically divergent, hence needs regularization, as expected.

The general function $I(x,\kappa,\kappa',(l-l')^2)$, where $\kappa' = n\cdot l'$, involves no extra work, as it can be obtained from the $l' = 0$ case with the replacement

$$\begin{aligned} k &\to k - l', \qquad l \to l - l', \\ x &\to x - \kappa', \qquad \kappa \to \kappa - \kappa'. \end{aligned} \tag{A6}$$

This yields

$$I(x,\kappa,\kappa',(l-l')^2)=\frac{N_c\omega^2\theta[(x-\kappa')(\kappa-x)]}{4\pi^2f^2|\kappa-\kappa'|}\times\int_0^\infty du\times\frac{1}{u+w^2+\frac{x-\kappa'}{\kappa-\kappa'}(1-\frac{x-\kappa'}{\kappa-\kappa'})(l-l')^2}. \tag{A7}$$

An important consequence of Lorentz invariance is *polynomiality* [1]. We verify it by introducing the variable $\nu=(x-\kappa')/(\kappa-\kappa')$, when $I(x,\kappa,\kappa',(l-l')^2)$ becomes a function of ν divided by $|\kappa-\kappa'|$. We obtain (assuming for definiteness $\kappa>\kappa'$)

$$\int_{-1}^1 dx I(x,\kappa,\kappa',(l-l')^2)x^n=\int_0^1 d\nu f(\nu)[\kappa'+\nu(\kappa-\kappa')]^n, \tag{A8}$$

which results in a polynomial in κ and κ' of the order at most n. The first few moments have the explicit form

$$\int_{-1}^1 dx I(x,\kappa,\kappa',\tau)=\frac{N_c\omega^2\tau}{4\pi^2f^2}\int_0^\infty du\frac{2\log(\frac{\sqrt{4A+1}-1}{\sqrt{4A+1}+1})}{\sqrt{4A+1}},$$
$$\int_{-1}^1 dx I(x,\kappa,\kappa',\tau)x=\frac{N_c\omega^2\tau}{4\pi^2f^2}\int_0^\infty du\frac{(\kappa+\kappa')\log(\frac{\sqrt{4A+1}-1}{\sqrt{4A+1}+1})}{\sqrt{4A+1}},$$
$$\int_{-1}^1 dx I(x,\kappa,\kappa',\tau)x^2=\frac{N_c\omega^2\tau}{4\pi^2f^2}\int_0^\infty du\times\frac{(4A+1)(\kappa-\kappa')^2-\sqrt{4A+1}\log(\frac{\sqrt{4A+1}+1}{\sqrt{4A+1}-1})((2A+1)\kappa^2-4A\kappa'\kappa+(2A+1)(\kappa')^2)}{4A+1}, \tag{A9}$$

where $A=(u+\omega^2)/\tau$ and $\tau=(l-l')^2$.

In the literature the D-term is by definition the two-point function in the t-channel [19]. It originates from the diagram with the contact pion-quark term as well as from the reduced three-point diagram, where by "reduction" one means the replacement of k^2 and $k\cdot l$ pieces appearing in the numerator from the trace factor, in terms of the inverse scalar propagators. The two-point functions in the s-channel (resulting from the reduction of the three-point function) are traditionally treated as singular parts of the double distributions.

2. Three-point functions

For the three-point functions we proceed analogously, now with three scalar propagators. We need to take into account the kinematics of the *direct* and *crossed* diagrams of Fig. 1. We first analyze in detail the three-point function resulting from the direct diagram (a), since the case of the crossed diagram is obtained via a simple kinematic transformation. We have

$$J(x,q\cdot n,p\cdot n,q^2,p^2,p\cdot q)=\frac{4N_c\omega^2}{f^2}\int\frac{d^4k}{(2\pi)^4}\delta(k\cdot n-x)S_kS_{k+q}S_{bk-p}$$
$$=4N_c\omega^2f^2\int\frac{d^4k}{(2\pi)^4}\int\frac{d\lambda}{2\pi}e^{i\lambda(k\cdot n-x)}\int_0^\infty da\int_0^\infty db\int_0^\infty dc e^{-a(k^2+\omega^2)-b((k+q)^2+\omega^2)-c((k-p)^2+\omega^2)}. \tag{A10}$$

Shifting the integration variable, $k'=k+(\beta q-\gamma p-i\lambda n/2)/(\alpha+\beta+\gamma)$, and carrying over the d^4k' integration yields

$$J=\frac{N_c\omega^2}{4\pi^2f^2}\int_0^\infty da\int_0^\infty db\int_0^\infty dc\frac{1}{(a+b+c)^2}\delta\Big(x-\frac{cp\cdot n-bq\cdot n}{a+b+c}\Big)$$
$$\times e^{-(a+b+c)\omega^2-b(a+c)/(a+b+c)q^2-c(a+b)/(a+b+c)p^2-2bc/(a+b+c)p\cdot q}. \tag{A11}$$

Next, we change the variables into

$$s=a+b+c,\qquad y=\frac{b}{s},\qquad z=\frac{c}{s}. \tag{A12}$$

Note that since $a,b,c\geq 0$, we get $0\leq y,z\leq 1$ and also $y+z\leq 1$. The substitution and integration over s yields

$$J = \frac{N_c\omega^2}{4\pi^2 f^2}\int_0^1 dy\int_0^1 dz\frac{\theta(1-y-z)\delta(x-zp\cdot n+yq\cdot n)}{\omega^2+y(1-y)q^2+z(1-z)p^2+2yzp\cdot q}. \tag{A13}$$

We note that polynomiality is obvious from this form, as multiplication by the power x^n is equivalent to the multiplication by the factor $(zp\cdot n - yq\cdot n)^n$. In the chiral limit of $m_\pi = 0$ the first few moments are relatively simple:

$$\begin{aligned}
\int_0^1 dxJ &= \frac{N_c\omega^2}{4\pi^2 f^2 t}2\left[\arctan\left(\frac{\sqrt{t}}{\sqrt{4w^2-t}}\right)\right]^2,\\
\int_0^1 dxJx &= \frac{N_c\omega^2}{4\pi^2 f^2 t^{3/2}}2\left(\sqrt{t}\left[\arctan\left(\frac{\sqrt{t}}{\sqrt{4w^2-t}}\right)\right]^2 - \sqrt{4w^2-t}(\zeta-2)\arctan\left(\frac{\sqrt{t}}{\sqrt{4w^2-t}}\right) + \sqrt{t}(\zeta-2)\right),\\
\int_0^1 dxJx^2 &= \frac{N_c\omega^2}{4\pi^2 f^2 t^2}\left[t(\zeta(\zeta+3)-7) + \arctan\left(\frac{\sqrt{t}}{\sqrt{4w^2-t}}\right)\right.\\
&\quad\left.\times\left(\sqrt{t}\sqrt{4w^2-t}(6-\zeta(\zeta+2)) + 2(t-2w^2(\zeta-1))\arctan\left(\frac{\sqrt{t}}{\sqrt{4w^2-t}}\right)\right)\right].
\end{aligned} \tag{A14}$$

We can rewrite Eq. (A13) as

$$\begin{aligned}
\mathcal{F}(z,y) &= \frac{N_c\omega^2}{4\pi^2 f^2}\frac{\theta(1-y-z)}{\omega^2 - y(1-y-z)t - z(1-z)m_\pi^2},\\
J(x) &= \int_0^1 dy\int_0^1 dz\,\delta(x-z-y\zeta)\mathcal{F}(z,y),
\end{aligned} \tag{A15}$$

where we have used the kinematics (2.1). The curly $\mathcal{F}$ denotes the *double distribution*.

Let us denote

$$\mathcal{D} = \omega^2 - y(1-y-z)t - z(1-z)m_\pi^2. \tag{A16}$$

For the GPD of the pion, due to the crossing symmetry, one may assume $0 \le \zeta \le 1$. Next, we perform the z integration, which sets

$$z = x - y\zeta. \tag{A17}$$

The distributions in Eq. (A13) give the following limits for the y integration:

$$\begin{aligned}
J = \frac{N_c\omega^2}{4\pi^2 f^2}\left(\theta[x(\zeta-x)]\int_0^{x/\zeta} + \theta[(x-\zeta)(1-x)]\right.\\
\left.\times\int_0^{(1-x)/(1-\zeta)}\right)\frac{dy}{\mathcal{D}},
\end{aligned} \tag{A18}$$

with the first term having the support $x \in [0, \zeta]$, and the second $x \in [\zeta, 1]$. The function $F(x)$ is continuous, but the derivative $dF(x)/dx$ is discontinuous at the points $x = 0, \zeta, 1$. The double distribution is *München-symmetric* [95], i.e., $\mathcal{F}(z,y) = \mathcal{F}(z, 1-y-z)$. This feature is related to the crossing symmetry, holding for identical particles.

The result for the crossed diagram (see Fig. 1) is obtained from the above result for the direct diagram with the replacement $p \to -p - q$. Replacing correspondingly $x \to \zeta - x$ and performing the München transformation [95]

$$z \to z, \qquad y \to 1-y-z, \tag{A19}$$

we find that $\mathcal{D}$ is *invariant* under this joint transformation. The function $\delta(x-z-y\zeta)$ is also invariant under these combined two transformations. Finally, the support is invariant, since

$$\begin{aligned}
&\theta(1-y-z)\theta[y(1-y)]\theta[z(1-z)]\\
&\quad\to \theta(y)\theta[(1-y-z)(y+z)]\theta[z(1-z)]\\
&\quad= \theta(1-y-z)\theta[y(1-y]\theta[z(1-z)],
\end{aligned} \tag{A20}$$

where the equality in the above formula is an algebraic identity. Therefore the crossed diagram is related to the direct diagram as follows:

$$J^{\text{crossed}}(x,\zeta) = J^{\text{direct}}(\zeta - x, \zeta). \tag{A21}$$

The support of the crossed diagram reflects the support of the direct diagram, i.e., $x \in [-1+\zeta, \zeta]$.

APPENDIX B: THE TWO- AND THREE-POINT FUNCTIONS IN THE SPECTRAL QUARK MODEL

According to the general rule, in SQM one appends the formulas with the spectral integration $\int_C d\omega\omega^2\rho(\omega)$. The results below are for the meson-dominance model.

1. The two-point function

We assume $\kappa' \le \kappa$. The spectral integration yields

$$\begin{aligned}
I_{\text{SQM}}(x,\kappa,\kappa',l^2) &= \int_C d\omega\omega^2\rho(\omega)I(x,\kappa,\kappa',l^2)\\
&= \frac{\theta[(x-\kappa')(\kappa-x)]}{(\kappa-\kappa')[1+4\frac{x-\kappa'}{\kappa-\kappa'}(1-\frac{x-\kappa'}{\kappa-\kappa'})\frac{l^2}{M_V^2}]^{3/2}},
\end{aligned} \tag{B1}$$

where we have used the relation

$$M_V^2 = 24\pi^2 f^2/N_c. \tag{B2}$$

The integration over x yields the form factor

$$\int dx I_{\rm SQM}(x,\kappa,\kappa',l^2)=\frac{M_V^2}{M_V^2+l^2}. \tag{B3}$$

In agreement with polynomiality, this form factor is independent of the value of κ or κ'. Note that the vector-meson dominance is readily obtained. Similarly,

$$\int dx I_{\rm SQM}(x,\kappa,\kappa',l^2)x=\frac{M_V^2}{M_V^2+l^2}\frac{\kappa+\kappa'}{2}. \tag{B4}$$

2. The three-point function

For simplicity in this appendix we work in the chiral limit. In this case the double distribution becomes

$$\mathcal{F}_{\omega}(z,y;t)=\frac{N_c\omega^2}{4\pi^2f^2}\frac{\theta(1-y-z)}{\omega^2-y(1-y-z)t}, \tag{B5}$$

and the subsequent spectral integration yields (again we only multiply by ω^2 and leave out other factors)

$$\mathcal{F}_{\rm SQM}(z,y;t)=\int_C d\omega\rho(\omega)\mathcal{F}_{\omega}(z,y;t)=\frac{N_c}{4\pi^2f^2}\frac{\theta(1-y-z)}{(1-\frac{4y(1-y-z)t}{M_V^2})^{5/2}}. \tag{B6}$$

Let us introduce the short-hand notation

$$\begin{aligned}\chi_2&=\frac{2(x-1)[3(\zeta-1)M_V^2+t(x-1)^2]}{[(\zeta-1)M_V^2+t(x-1)^2]^2},\\ \chi_1&=\frac{(x(\zeta-2)+\zeta)(3M_V^2(\zeta-1)\zeta^2+t((\zeta^2+8\zeta-8)x^2+2(4-5\zeta)\zeta x+\zeta^2))}{((\zeta-1)M_V^2+t(x-1)^2)^2(\zeta^2+\frac{4tx(x-\zeta)}{M_V^2})^{3/2}}+\frac{1}{2}\chi_2.\end{aligned} \tag{B7}$$

Then, for the case $\zeta\geq 0$,

$$J_{\rm SQM}(x,\zeta;t)=(\theta[x(\zeta-x)]\chi_1+\theta[(1-x)(x-\zeta)]\chi_2). \tag{B8}$$

The function satisfies $J_{\rm SQM}(0,\zeta;t)=J_{\rm SQM}(1,\zeta;t)=0$. The value at the matching point $x=\zeta$ is

$$J_{\rm SQM}(\zeta,\zeta;t)=\frac{2(3M_V^2+t(\zeta-1))}{(M_V^2+t(\zeta-1))^2}. \tag{B9}$$

The integration over x produces a ζ-independent (as required by polynomiality) form factor,

$$\int_0^1 dx J_{\rm SQM}(x,\zeta;t)=\frac{2}{M_V^2-t}-\frac{\log(1-\frac{t}{M_V^2})}{t}. \tag{B10}$$

Similarly,

$$\int_0^1 dx J_{\rm SQM}(x,\zeta;t)x=\frac{\zeta}{M_V^2-t}-\frac{\log(1-\frac{t}{M_V^2})}{t}. \tag{B11}$$

For the special case of $t=0$ Eq. (B8) reduces to the very simple expression

$$J_{\rm SQM}(x,\zeta;0)=\frac{6}{M_V^2}\left(\theta[x(\zeta-x)]\frac{x}{\zeta}+\theta[(1-x)(x-\zeta)]\times\frac{x-1}{\zeta-1}\right), \tag{B12}$$

which is a triangle of area $3/M_V^2=N_c/(8\pi^2f^2)$.

For the case $\zeta=0$ we have

$$J_{\rm SQM}(x,0;t)=\frac{(3M_V^2-t(1-x)^2)(1-x)}{(M_V^2-t(1-x)^2)^2}. \tag{B13}$$

APPENDIX C: THE TWO- AND THREE-POINT FUNCTIONS IN THE NJL MODEL

Operationally, the calculation in the NJL model with the regularization [(4.1)] amounts to taking the generic expressions (A7) and (A18), replacing $\omega^2\to M^2+\Lambda^2$ *in the denominators*, carrying out the integrations, and finally applying (4.1). We work in the chiral limit.

1. The two-point function

Through the use of Eq. (4.2) we arrive immediately at the formula (for $\kappa\geq\kappa'$)

$$I_{\rm NJL}(x,\kappa,\kappa',0)=\frac{\theta[(x-\kappa')(\kappa-x)]}{\kappa-\kappa'}. \tag{C1}$$

2. The three-point function

We find

$$J_{\rm NJL}(x,\zeta;m_\pi=0;\Lambda)=-\frac{N_c M^2}{8\pi^2 f^2}\left[\frac{2\log\left(\frac{\sqrt{-t}(x-1)+\sqrt{-t(x-1)^2-4(\zeta-1)(M^2+\Lambda^2)}}{\sqrt{-t(x-1)^2-4(\zeta-1)(M^2+\Lambda^2)}-\sqrt{-t}(x-1)}\right)\theta((1-x)(x-\zeta))}{\sqrt{-t}\sqrt{-t(x-1)^2-4(\zeta-1)(M^2+\Lambda^2)}}\right.$$
$$\left.+\frac{\left(\log\left(\frac{\sqrt{-t}(x-1)+\sqrt{-t(x-1)^2-4(\zeta-1)(M^2+\Lambda^2)}}{\sqrt{-t(x-1)^2-4(\zeta-1)(M^2+\Lambda^2)}-\sqrt{-t}(x-1)}\right)+\log\left(\frac{\sqrt{-t(x-1)^2-4(\zeta-1)(M^2+\Lambda^2)}\zeta+\sqrt{-t}(x(\zeta-2)+\zeta)}{\zeta\sqrt{-t(x-1)^2-4(\zeta-1)(M^2+\Lambda^2)}-\sqrt{-t}(x(\zeta-2)+\zeta)}\right)\right)\theta(x(\zeta-x))}{\sqrt{-t}\sqrt{-t(x-1)^2-4(\zeta-1)(M^2+\Lambda^2)}}\right], \tag{C2}$$

and

$$J_{\rm NJL}(x,\zeta;m_\pi=0)=J_{\rm NJL}(x,\zeta;m_\pi=0;\Lambda)|_{\rm reg}. \tag{C3}$$

Polynomiality follows from the fact that the expressions are derived from the double distributions (A15) and the distributive nature of the regularization prescription ((4.1)). By *distributive* we mean that it is a sum over quark masses or the integral over ω of the formal expressions for I and J.

APPENDIX D: THE GRAVITATIONAL FORM FACTORS

The gravitational form factors of the pion [55] are defined through the matrix element of the energy-momentum tensor,

$$\langle\pi^b(p+q)\mid\theta^{\mu\nu}(0)\mid\pi^a(p)\rangle = \frac{\delta^{ab}}{2}((g^{\mu\nu}q^2-q^\mu q^\nu)\theta_1(q^2) + (2p+q)^\mu(2p+q)^\nu\theta_2(q^2)). \tag{D1}$$

They satisfy the low-energy theorem $\theta_1(0)-\theta_2(0)=\mathcal{O}(m_\pi^2)$ [55]. The leading-N_c quark-model evaluation amounts to computing the diagrams of Figs. 1 and 2 with the pion gravitational vertex

$$\theta^{\mu\nu}(k+q,k)=\frac{1}{4}((2k+q)^\mu\gamma^\nu+(2k+q)^\nu\gamma^\mu) - \frac{1}{2}g^{\mu\nu}(2\not{k}+\not{q}-\omega). \tag{D2}$$

The results of the calculation in SQM is Eq. (3.5). Equation (2.10) follows from considering the matrix element of $n_\mu\theta^{\mu\nu}n_\nu$. Then

$$\langle\pi^b(p+q)\mid n_\mu\theta^{\mu\nu}(0)n_\nu\mid\pi^a(p)\rangle = \delta^{ab}\frac{1}{2}[\zeta^2\theta_1(q^2)+(2-\zeta)^2\theta_2(q^2)]. \tag{D3}$$

The vertex becomes

$$n_\mu\theta^{\mu\nu}(k+q,k)n_\nu=(x-\zeta/2)\gamma\cdot n. \tag{D4}$$

We notice it is the same vertex as in the evaluation of the GPD's multiplied by $(x-\zeta/2)$. Upon passing to the symmetric notation Eq. (2.10) follows.

APPENDIX E: END-POINT ANALYSIS FOR THE PDA

Here we derive the formulas used in the main text of Sec. V E for the PDA and correct a mistake in expressions of our previous work [27,31]. Right at the end points, $x=0,1$, the series (5.18) diverges since $C_{2k}^{3/2}(\pm1)=\frac{1}{2}(2k+1)(2k+2)$, meaning a nonuniform convergence as $x\to0$ or $x\to1$ as well as the large-n dominance of the end-point behavior. In this limit we have [85]

$$\left(\frac{\alpha(Q)}{\alpha(Q_0)}\right)^{\gamma_n^{(0)}/(2\beta_0)}\sim n^{-8r(Q_0,Q)}e^{2(3-4\gamma)r(Q_0,Q)}. \tag{E1}$$

Only even-n terms contribute in Eq. (5.18), hence we impose this condition for integer n and then extend n to real values. The summation in Eq. (5.18) is then replaced with an integral,

$$\phi(x,Q)\sim\frac{1}{2}8xe^{(3/4-\gamma)a}\int_0^\infty dn C_n^{3/2}(2x-1)n^{-a-1}, \tag{E2}$$

where the factor of $1/2$ comes from the summation over even n only, and

$$a=8r(Q_0,Q). \tag{E3}$$

The Gegenbauer polynomials $C_n^{3/2}(\xi)$ in the variable $\xi=2x-1$ satisfy the differential equation [96]

$$(1-\xi^2)y''(\xi)-4\xi y'(\xi)+n(n+3)y(\xi)=0, \tag{E4}$$

which upon the substitution

$$y(\xi)=\frac{u(\xi)}{1-\xi^2}, \tag{E5}$$

transforms into a Schrödinger-like equation at zero energy,

$$u''(\xi)+\frac{n^2+3n+2}{1-\xi^2}u(\xi)=0. \tag{E6}$$

Here the interval of interest, $-1\le\xi\le1$, corresponds to the classically allowed region and the potential is attractive. In the large-n limit the solution oscillates rapidly and a semiclassical WKB approximation [97] might be used. Here in order to analyze the limit $x\to0$ we consider the differential equation, Eq. (E6), which in the limit $x\to0$ and $n\gg1$ transforms into a zero-energy Coulomb-like

problem. Its solution can be generally written in terms of the Bessel functions,

$$C_n^{3/2}(2x-1) = \frac{c_1 J_1(2n\sqrt{x}) + c_2 Y_1(2n\sqrt{x})}{\sqrt{x}}, \tag{E7}$$

where actually $c_2 = 0$, since the Gegenbauer polynomials are regular at the end point $x = 0$. The undetermined constant c_1 may be obtained by matching the small argument expansion $J_1(z) = z/2 + \ldots$ to the value $C_n^{3/2}(1) \sim \frac{n^2}{2}$, yielding for $n \gg 1$ and $x \to 0$ the formula

$$C_n^{3/2}(2x-1) \sim \frac{n}{2\sqrt{x}} J_1(2n\sqrt{x}). \tag{E8}$$

As we see in the low-x and large-n limit there is a scaling behavior of the Gegenbauer polynomials,

$$C_n^{3/2}(x) \sim nF(n\sqrt{x})/\sqrt{x}. \tag{E9}$$

From Eq. (E2) it is now clear that this translates into the low-x scaling behavior

$$\phi(x, Q) \sim x^{a/2} e^{(3/4-\gamma)a} \int_0^\infty dt F(t) t^{-a}. \tag{E10}$$

Evaluation of the integral and collecting the factors yields Eq. (5.26).

[1] X.-D. Ji, J. Phys. G **24**, 1181 (1998).
[2] A. V. Radyushkin, arXiv:hep-ph/0101225.
[3] K. Goeke, M. V. Polyakov, and M. Vanderhaeghen, Prog. Part. Nucl. Phys. **47**, 401 (2001).
[4] M. Diehl, Phys. Rep. **388**, 41 (2003).
[5] X. Ji, Annu. Rev. Nucl. Part. Sci. **54**, 413 (2004).
[6] A. V. Belitsky and A. V. Radyushkin, Phys. Rep. **418**, 1 (2005).
[7] T. Feldmann, Eur. J. Phys. Special Topics **140**, 135 (2007).
[8] S. Boffi and B. Pasquini, arXiv:0711.2625.
[9] A. V. Belitsky, X.-d. Ji, and F. Yuan, Phys. Rev. D **69**, 074014 (2004).
[10] J. C. Collins, L. Frankfurt, and M. Strikman, Phys. Rev. D **56**, 2982 (1997).
[11] A. P. Szczepaniak, J. T. Londergan, and F. J. Llanes-Estrada, arXiv:0707.1239.
[12] M. Burkardt and S. Dalley, Prog. Part. Nucl. Phys. **48**, 317 (2002).
[13] P. Hagler, Proc. Sci., LATTICE 2007 (2007) 013) [arXiv:0711.0819].
[14] S. Ahmad, H. Honkanen, S. Liuti, and S. K. Taneja, arXiv:0708.0268.
[15] M. Diehl, A. Manashov, and A. Schafer, Phys. Lett. B **622**, 69 (2005).
[16] J.-W. Chen, W. Detmold, and B. Smigielski, Phys. Rev. D **75**, 074003 (2007).
[17] N. Kivel and M. V. Polyakov, arXiv:0707.2208.
[18] A. V. Radyushkin, Phys. Rev. D **59**, 014030 (1998).
[19] M. V. Polyakov and C. Weiss, Phys. Rev. D **60**, 114017 (1999).
[20] B. Pire, J. Soffer, and O. Teryaev, Eur. Phys. J. C **8**, 103 (1999).
[21] P. V. Pobylitsa, Phys. Rev. D **65**, 077504 (2002).
[22] M. V. Polyakov, Nucl. Phys. **B555**, 231 (1999).
[23] R. M. Davidson and E. Ruiz Arriola, Phys. Lett. B **348**, 163 (1995).
[24] H. Weigel, E. Ruiz Arriola, and L. P. Gamberg, Nucl. Phys. **B560**, 383 (1999).
[25] A. Van Dyck, T. Van Cauteren, and J. Ryckebusch, arXiv:0710.2271.
[26] C. V. Christov *et al.*, Prog. Part. Nucl. Phys. **37**, 91 (1996).
[27] E. Ruiz Arriola, Acta Phys. Pol. B **33**, 4443 (2002).
[28] E. Ruiz Arriola, arXiv:hep-ph/0107087.
[29] E. Ruiz Arriola and W. Broniowski, Phys. Rev. D **67**, 074021 (2003).
[30] R. M. Davidson and E. Ruiz Arriola, Acta Phys. Pol. B **33**, 1791 (2002).
[31] E. Ruiz Arriola and W. Broniowski, Phys. Rev. D **66**, 094016 (2002).
[32] W. Broniowski and E. Ruiz Arriola, Phys. Lett. B **574**, 57 (2003).
[33] B. Pire and L. Szymanowski, Phys. Rev. D **71**, 111501 (2005).
[34] B. Pire and L. Szymanowski, Phys. Lett. B **622**, 83 (2005).
[35] W. Broniowski and E. R. Arriola, Phys. Lett. B **649**, 49 (2007).
[36] I. V. Anikin, A. E. Dorokhov, A. E. Maksimov, L. Tomio, and V. Vento, Nucl. Phys. **A678**, 175 (2000).
[37] I. V. Anikin, A. E. Dorokhov, A. E. Maksimov, and L. Tomio, Phys. At. Nucl. **63**, 489 (2000).
[38] A. E. Dorokhov and L. Tomio, arXiv:hep-ph/9803329.
[39] A. E. Dorokhov and L. Tomio, Phys. Rev. D **62**, 014016 (2000).
[40] M. V. Polyakov and C. Weiss, Phys. Rev. D **59**, 091502 (1999).
[41] M. Praszalowicz and A. Rostworowski, Acta Phys. Pol. B **34**, 2699 (2003).
[42] A. Bzdak and M. Praszalowicz, Acta Phys. Pol. B **34**, 3401 (2003).
[43] S. Noguera and V. Vento, Eur. Phys. J. A **28**, 227 (2006).
[44] A. P. Bakulev, R. Ruskov, K. Goeke, and N. G. Stefanis, Phys. Rev. D **62**, 054018 (2000).
[45] H.-M. Choi, C.-R. Ji, and L. S. Kisslinger, Phys. Rev. D **64**, 093006 (2001).
[46] H.-M. Choi, C.-R. Ji, and L. S. Kisslinger, Phys. Rev. D **66**, 053011 (2002).
[47] A. Mukherjee, I. V. Musatov, H. C. Pauli, and A. V. Radyushkin, Phys. Rev. D **67**, 073014 (2003).
[48] B. C. Tiburzi and G. A. Miller, Phys. Rev. D **67**, 013010 (2003).

[49] B. C. Tiburzi and G. A. Miller, Phys. Rev. D **67**, 113004 (2003).
[50] A. V. Radyushkin, Phys. Lett. B **449**, 81 (1999).
[51] F. Bissey, J. R. Cudell, J. Cugnon, J. P. Lansberg, and P. Stassart, Phys. Lett. B **587**, 189 (2004).
[52] L. Theussl, S. Noguera, and V. Vento, Eur. Phys. J. A **20**, 483 (2004).
[53] J. S. Conway *et al.*, Phys. Rev. D **39**, 92 (1989).
[54] E. M. Aitala *et al.* (E791), Phys. Rev. Lett. **86**, 4768 (2001).
[55] J. F. Donoghue and H. Leutwyler, Z. Phys. C **52**, 343 (1991).
[56] G. A. Miller, Phys. Rev. Lett. **99**, 112001 (2007).
[57] M. Diehl, T. Gousset, B. Pire, and O. Teryaev, Phys. Rev. Lett. **81**, 1782 (1998).
[58] E. Ruiz Arriola, Phys. Lett. B **264**, 178 (1991).
[59] E. R. Arriola, W. Broniowski, and B. Golli, Phys. Rev. D **76**, 014008 (2007).
[60] X.-D. Ji, Phys. Rev. D **52**, 271 (1995).
[61] G. Altarelli and G. Parisi, Nucl. Phys. B **126**, 298 (1977).
[62] P. J. Sutton, A. D. Martin, R. G. Roberts, and W. J. Stirling, Phys. Rev. D **45**, 2349 (1992).
[63] M. Gluck, E. Reya, and I. Schienbein, Eur. Phys. J. C **10**, 313 (1999).
[64] G. Martinelli and C. T. Sachrajda, Nucl. Phys. **B306**, 865 (1988).
[65] C. Best *et al.*, Phys. Rev. D **56**, 2743 (1997).
[66] S. Capitani *et al.*, Phys. Lett. B **639**, 520 (2006).
[67] H. B. Meyer and J. W. Negele, Phys. Rev. D **77**, 037501 (2008).
[68] S. Dalley, Phys. Rev. D **64**, 036006 (2001).
[69] M. Burkardt and S. K. Seal, Phys. Rev. D **64**, 111501 (2001).
[70] K. Wijesooriya, P. E. Reimer, and R. J. Holt, Phys. Rev. C **72**, 065203 (2005).
[71] S. Dalley and B. van de Sande, Phys. Rev. D **67**, 114507 (2003).
[72] M. Gluck, E. Reya, and I. Schienbein, Eur. Phys. J. C **10**, 313 (1999).
[73] I. V. Anikin, A. E. Dorokhov, and L. Tomio, Phys. Lett. B **475**, 361 (2000).
[74] A. E. Dorokhov, JETP Lett. **77**, 63 (2003).
[75] A. P. Bakulev, S. V. Mikhailov, and N. G. Stefanis, Phys. Lett. B **578**, 91 (2004).
[76] A. P. Bakulev, S. V. Mikhailov, and N. G. Stefanis, Phys. Rev. D **73**, 056002 (2006).
[77] A. P. Bakulev, S. V. Mikhailov, A. V. Pimikov, and N. G. Stefanis, arXiv:0710.2275.
[78] G. P. Lepage and S. J. Brodsky, Phys. Rev. D **22**, 2157 (1980).
[79] D. Mueller, Phys. Rev. D **51**, 3855 (1995).
[80] A. Schmedding and O. I. Yakovlev, Phys. Rev. D **62**, 116002 (2000).
[81] J. Gronberg *et al.* (CLEO), Phys. Rev. D **57**, 33 (1998).
[82] L. Del Debbio, M. Di Pierro, and A. Dougall, Nucl. Phys. B, Proc. Suppl. **119**, 416 (2003).
[83] V. M. Braun *et al.*, Phys. Rev. D **74**, 074501 (2006).
[84] M. A. Donnellan *et al.*, Proc. Sci., LATTICE 2007 (2007) 369 [arXiv:0710.0869].
[85] E. Ruiz Arriola and W. Broniowski, Phys. Rev. D **70**, 034012 (2004).
[86] S. Dalley, Phys. Lett. B **570**, 191 (2003).
[87] S. Dalley, Few-Body Syst. **36**, 69 (2005).
[88] D. Mueller, D. Robaschik, B. Geyer, F. M. Dittes, and J. Horejsi, Fortschr. Phys. **42**, 101 (1994).
[89] X.-D. Ji, Phys. Rev. D **55**, 7114 (1997).
[90] A. V. Radyushkin, Phys. Rev. D **56**, 5524 (1997).
[91] J. Blumlein, B. Geyer, and D. Robaschik, Phys. Lett. B **406**, 161 (1997).
[92] K. J. Golec-Biernat and A. D. Martin, Phys. Rev. D **59**, 014029 (1998).
[93] N. Kivel and L. Mankiewicz, Nucl. Phys. **B557**, 271 (1999).
[94] N. Kivel and L. Mankiewicz, Phys. Lett. B **458**, 338 (1999).
[95] L. Mankiewicz, G. Piller, and T. Weigl, Eur. Phys. J. C **5**, 119 (1998).
[96] M. Abramowitz and I. A. Stegun, *Handbook of Mathematical Functions* (Dover Publications, New York, 1964).
[97] A. Galindo and P. Pascual, *Quantum Mechanics* (Springer, New York, 1991).